2011

Impurity And Interdiffusion In The Magnesium-aluminum System

Sarah Tiffany Brennan
University of Central Florida

IMPURITY AND INTERDIFFUSION IN THE MAGNESIUM-ALUMINUM SYSTEM

by

SARAH TIFFANY BRENNAN
B.S. University of Central Florida, 2009

A thesis submitted in partial fulfillment of the requirements
for the degree of Master of Science
in the Department of Mechanical, Materials, and Aerospace Engineering
in the College of Engineering and Computer Science
at the University of Central Florida
Orlando, Florida

Summer Term
2011

Major Professor: Yong-ho Sohn

ABSTRACT

Magnesium alloys offer a base of lightweight engineering materials for electronic, military and transportation applications where weight reduction is crucial for higher efficiency. Understanding fundamental diffusion behavior in Mg alloys elicits better materials properties through the optimization of processing techniques and heat treatments, whose material responses are affected by diffusion. The main objective of this study is to provide a clear, comprehensive description of the diffusion behavior in the technically important magnesium-aluminum binary metallic system.

In this study, diffusion in the Mg-Al system was observed through solid diffusion couples and thin film specimens in the temperature range of 673-523K. The formation and growth of the intermetallic phases, β-Mg_2Al_3 and γ-$Mg_{17}Al_{12}$, and the absence of the ε-$Mg_{23}Al_{30}$ phase was observed. The β-Mg_2Al_3 phase grew thicker, had higher parabolic growth constants and lower activation energy for growth. Concentration-dependent interdiffusion coefficients were determined using the Boltzmann-Matano method. Interdiffusion in the β-Mg_2Al_3 phase was the highest, followed by the γ-$Mg_{17}Al_{12}$ phase, the Al solid solution and the Mg solid solution. Intrinsic diffusion coefficients at the marker plane composition of 38 at.% Mg in the β-Mg_2Al_3 were determined from Heumann's method for Mg and Al, for which Al was higher. Extrapolations of the impurity diffusion coefficients in both terminal solid solutions were made and compared to available literature data. The thermodynamic factor, tracer diffusivity and atomic

mobility of Mg and Al at the marker plane concentration were estimated using Mg activities in the β-Mg_2Al_3 available from literature.

The impurity diffusion of Al and self-diffusion of the stable isotope, ^{25}Mg, in polycrystalline Mg was measured from thin film specimens via depth profiling using secondary ion mass spectrometry. The Al impurity diffusion observed is compared to the extrapolations from the parallel interdiffusion study. The self-diffusion measurements are compared to reported literature values and were observed to be significantly higher. Several reasons for the observed difference in the magnitude of diffusivities are discussed.

This work is dedicated to my family and close friends, especially my mother. Thank you for your never-ending support, love and guidance.

ACKNOWLEDGMENTS

I would like to express my sincerest gratitude to my advisor, Dr. Yong-ho Sohn for his continued patience, guidance, support and encouragement. I also wish to thank the student research group under Dr. Sohn for their continuing support, critical discussions and encouragement. I want to thank my family and friends for their patience and support as well. I would also like to acknowledge the assistance of the staff at the Materials Characterization Facility at the University of Central Florida.

This research was sponsored by the U.S. Department of Energy, Assistant Secretary for Energy Efficiency and Renewable Energy, Office of Vehicle Technologies, as part of the Lightweight Materials Program. I would like to thank Dr. Nagraj Kulkarni from Oak Ridge National Laboratory, Dr. Jerry Hunter from Virginia Tech, and Mr. Andrew Warren, Mr. Ed Dein and Dr. Kevin Coffey from the University of Central Florida for their support and assistance with this work.

TABLE OF CONTENTS

LIST OF FIGURES

LIST OF TABLES

LIST OF ABBREVIATIONS AND ACRYONYMS

A_i	Accumulated intrinsic diffusion flux
a	Activity
β_i	Mobility of component i
C_i	Concentration of component i
D_i	Intrinsic diffusion coefficient of component i
$\widetilde{D}$	Binary interdiffusion coefficient
D_i^*	Tracer diffusion coefficient of component i
D_o	Pre-exponential factor for diffusion
$\widetilde{D}_{i,\Delta x}^{int}$	Integrated interdiffusion coefficient of component i
$\widetilde{D}_i^{eff}$	Average effective interdiffusion coefficient of component i
EPMA	Electron probe micro-analysis
$\tilde{J}_i$	Interdiffusion flux of component i
J_i	Intrinsic diffusion flux of component i
k_l	Linear intermetallic phase growth constant
k_p	Parabolic intermetallic phase growth constant
k_o	Pre-exponential factor for growth
N_i	Concentration of component i in mole fraction
OM	Optical microscopy
Φ	Thermodynamic factor
Q	Activation energy for diffusion
Q_k	Activation energy for intermetallic phase layer growth

R	Ideal gas constant (8.314 kJ/mole)
S	Vacancy wind factor, or Manning Factor
SEM	Scanning electron microscopy
SIMS	Secondary ion mass spectrometry
T	Temperature
μ_i	Chemical potential
μ_i^o	Standard chemical potential (at 298K and 1 atm)
v_k	Kirkendall plane velocity
V_m	Molar volume
x	position
x_m	Kirkendall marker plane position
x_o	Matano plane position
XEDS	X-ray energy dispersive spectroscopy
ZAF	Atomic number, absorption and fluorescence correction factor

1 INTRODUCTION

The necessity to increase efficiency through weight reduction has stimulated research in lightweight materials. Magnesium alloys and composites are extremely attractive lightweight materials for numerous electronic, military and transportation applications where weight reduction is crucial for safety and performance (Mordike & Ebert, 2001) (Luo, 2002) (Kulekci, 2008) (Urbance, Field, Kirchain, Roth, & Clark, 2002) (Cho, et al., 2009) (Zaludova, 2005) (Ye & Liu, 2004) (Bamberger & Dehm, 2008). Aside from their lightweight, Mg alloys also possess high specific strength, excellent castability, workability and machinability. The most commonly used Mg alloys are those based on the magnesium-aluminum (Mg-Al) system, such as the Mg alloy, AZ91, which has two main alloying additions, aluminum and zinc. In order to further advance the relevant properties of Mg alloys for widespread applications, an understanding of fundamental materials behavior, such as diffusion, is needed.

The materials phenomenon of diffusion plays an important role in alloy optimization and development. Knowledge of reliable diffusion properties in Mg alloys can aid in designing, processing, manufacturing, and understanding degradation of new and existing alloys. Despite the great potential for many applications, reports of diffusion properties for Mg and Mg-alloys are scarce and predate the recent interest. A compilation of most of the available tracer and self-diffusion data in Mg was provided by

Fujikawa in 1992 (Fujikawa S. , 1992). Recently, diffusion of rare-earth elements in Mg has been explored (Xu, Chumbley, Weigelt, & Laabs, 2001) (Zhang, Kevorkov, & Pekguleryuz, 2010) due to their ability to improve the strength and creep resistance of Mg alloys through precipitation hardening.

In this investigation, Mg-Al interdiffusion was examined by using solid-to-solid diffusion couples. The Mg-Al system is of great technical importance in both commercial Mg and Al alloys. Experimental observations and analysis were carried out with respect for previous studies on Mg-Al interdiffusion (Heumann & Kottmann, 1953) (Funamizu & Watanabe, 1972) (Tanguep Njiokep, Salomon, & Mehrer, 2001) wherein some discrepancies in microstructural features are identified, and the concentration-dependence of interdiffusion coefficients was not fully reported.

A study of the impurity diffusion of Al in polycrystalline Mg was also conducted in parallel utilizing the thin film method and depth profiling with secondary ion mass spectrometry (SIMS). Diffusion measurements with SIMS are advantageous because accurate measurements can be made with small diffusion distances, thus shortening the experimental annealing time and subsequent time spent obtaining the concentration profile, for example, in contrast to using the classical sectioning technique where carefully thinned slices of the sample are cut and individually analyzed.

The self-diffusion of the stable isotope, ^{25}Mg in polycrystalline Mg was also investigated via the use of thin film specimens and SIMS depth profiling.

The main objectives of these diffusion studies are

- To investigate the interdiffusion behavior of the Mg-Al system via solid diffusion couples to observe
    - Intermetallic phase layer formation and growth kinetics
    - Concentration-dependent interdiffusion behavior
    - Intrinsic diffusion behavior at the Kirkendall marker plane location
- To compare this studies results with previous studies on the Mg-Al system and clarify the discrepancies regarding the diffusion behavior of the system and observed microstructural features (marker plane and pores).
- To verify that utilizing SIMS for diffusion measurements in Mg systems is applicable and address issues associated with the measurements.
- To study the impurity diffusion of Al in polycrystalline Mg via SIMS depth profiling.
- To study the self-diffusion of the stable isotope ^{25}Mg in polycrystalline Mg, also using depth profiling with SIMS.

Finally, conclusions from all three studies are presented to encompass the growth and diffusion behavior in this exceptional, technically important binary metallic system.

2 LITERATURE REVIEW

2.1 Reactive Diffusion and Growth

Diffusion refers to the movement of atoms, ions or molecules in a gas, liquid or solid. Studying this movement of atoms allows for an understanding of certain material behaviors and properties related to kinetics phenomena and defect types and structures. Diffusion in solids involves the migration of atoms under a chemical potential gradient or, the force to cause intermixing. Diffusion can occur under a number of chemical potential gradients such as a concentration gradient, an electrical potential gradient, a thermal gradient or a stress gradient. This migration occurs in order to lower the free energy of the system to reach equilibrium. For the purposes of this document, only isothermal diffusion (concentration gradient) will be discussed. In this case, atoms migrate to decrease the concentration gradient by the thermally activated process of diffusion. This process is demonstrated in Figure 1 by a schematic of a diffusion couple experiment between two pure metals, A and B. A diffusion couple is made by joining two bars of two different metals or alloys together, providing close contact between the faces. The diffusion couple is then annealed at an elevated temperature for a period of time and then cooled to room temperature.

Knowledge of diffusion is the basis to understanding the various changes that can occur at elevated temperatures. Several materials phenomena such as precipitation, oxidation, creep, and the heat treatments of alloys are diffusion controlled. Knowledge

of diffusion, the migration of atoms, also gives insight into the study of defects in solids, such as voids and dislocations (Shewmon, 1989).

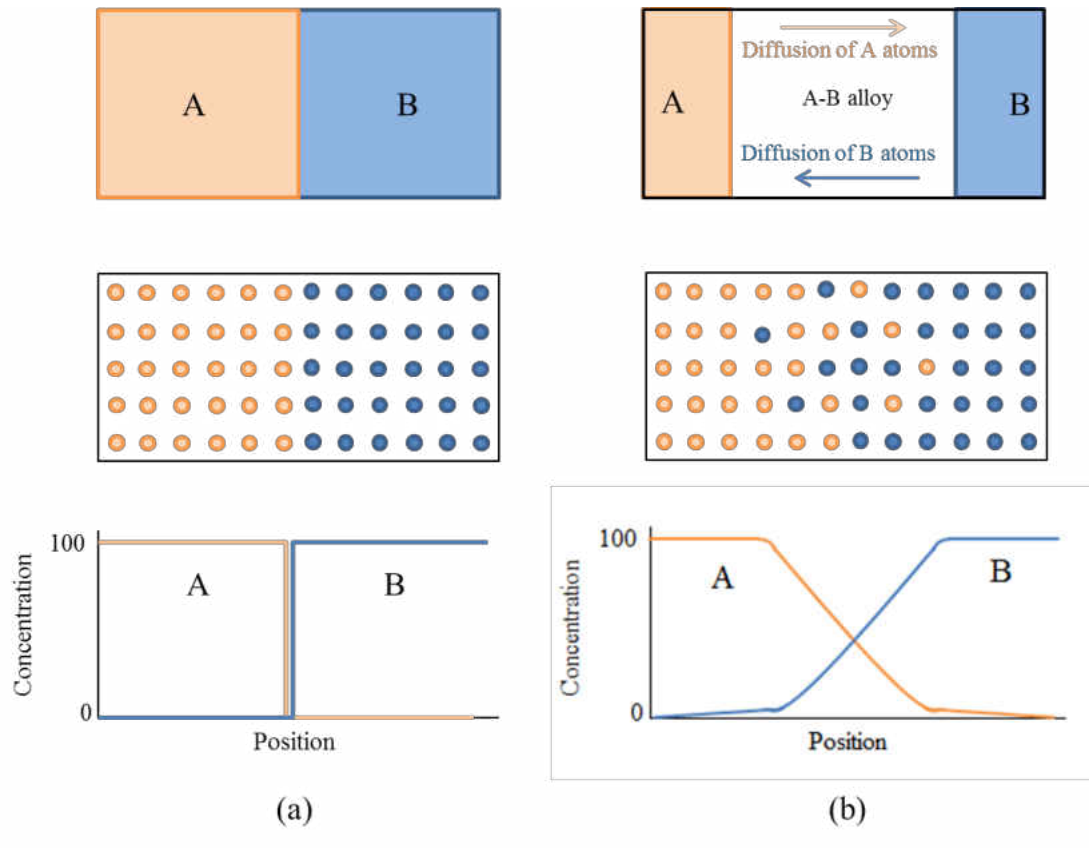

Figure 1: Schematic illustration of a binary diffusion couple of elements A and B (a) initial configuration before annealing, (b) mixing of A and B atoms due to diffusion after annealing.

Reactive diffusion is a physical-chemical process that results in a solid continuous compound layer forming at the initial interface between two or more substances. This layer formation and growth is due to continuous combination of the diffusion of atoms of

the bulk reactants and chemical reactions taking place at the interfaces with these diffusing atoms (Dybkov, 2002). These chemical reactions include:

- The transition of atoms of one substance through the interface from one phase to another
- The formation of molecules or ions by the redistribution of the electronic density of atomic orbitals
- The rearrangement of a crystal lattice of an initial phase into that of the chemical compound being formed.

Figure 2 conveys the case of a simple binary system with elemental substances, A and B, which forms only one intermetallic compound according to the equilibrium phase diagram. The intermetallic layer, A_mB_n, grows according to the rate of chemical reactions taking place at the interfaces of both A and B and the rate of diffusion of these atoms to the interfaces. There are two main growth regimes that can typically describe this growth process, the reaction controlled regime and the diffusion controlled regime.

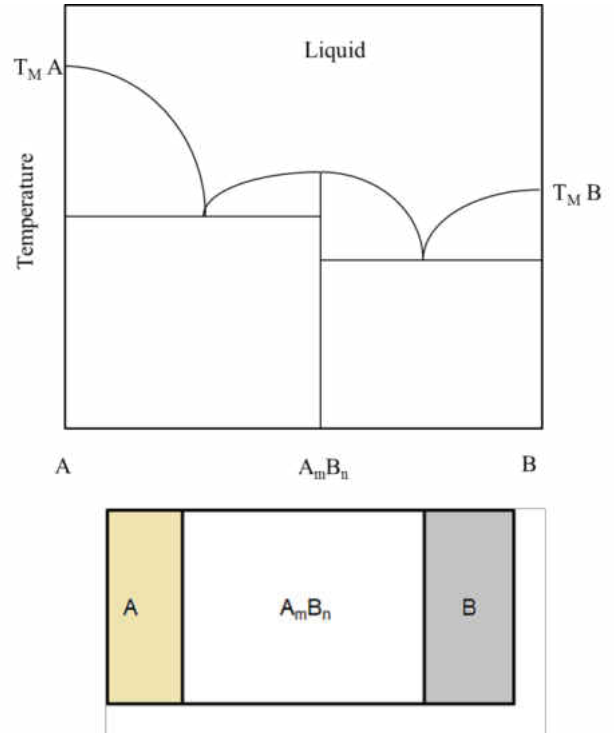

Figure 2: Schematic of an equilibrium phase diagram with one intermetallic compound and a diffusion couple with the resulting growth of the intermetallic compound after annealing.

Initially, when the growing intermetallic layer is very thin, there is a short diffusion path for the atoms to migrate across, allowing for essentially constant chemical reactivity at the interface. This regime is *reaction controlled*, and is only limited by the rate of chemical reactions. This initial growth regime is linear and can be described by

$$x = k_l t \tag{1}$$

where x is the layer thickness in meters, k_l is the linear growth constant in m/s and t is the annealing time in seconds.

The *diffusion controlled* regime is the other extreme. As a layer grows, the diffusion path for the supply atoms is increasing, essentially slowing the rate of the chemical reactions occurring. When the layer reaches a certain critical thickness, its growth becomes dependent on the rate of diffusion of the supply atoms through the layer and the effect of the rate of chemical reactions on its growth becomes negligible. The time dependence of the intermetallic layer thickness in the diffusion controlled regime can be described by the parabolic equation

$$x^2 = 2k_p t \tag{2}$$

where x (m) is the layer thickness, k_p (m^2/s) is the parabolic growth constant and t (s) is the time. Some theoretical analyses for layer growth of an intermetallic phase have been given by several investigators (Kidson, 1961) (Gibbs, 1966) (Kajihara, 2004) (Pretorius, Marais, & Theron, 1993). From these investigations, in summary, an intermediate phase layer will grow more rapidly as:

- the diffusion coefficient in the layer is larger,
- the diffusion coefficients in the surrounding phases are smaller,

- the homogeneity range of the phase in the equilibrium phase diagram is wider,
- the concentration range of the surrounding two-phase areas in the phase diagram is narrower,
- the heat of formation of the phase is higher, and
- the crystal structures between adjoining phases are similar.

These observations are not absolute, however; a phase may grow thicker and only follow one or two of these observations.

2.2 The Vacancy Mechanism of Diffusion and the Kirkendall Effect

Atoms in a crystal lattice oscillate around their equilibrium lattice positions, and on occasion, the oscillations are large enough for an atom to jump from its position. These atomic jumps give rise to the diffusion of atoms in solids. Not all crystal sites are occupied by atoms, however. Unoccupied lattice sites are called vacancies. The vacancy mechanism of diffusion, shown schematically in Figure 3, is an atom in a lattice site next to a vacancy jumping to fill the vacancy.

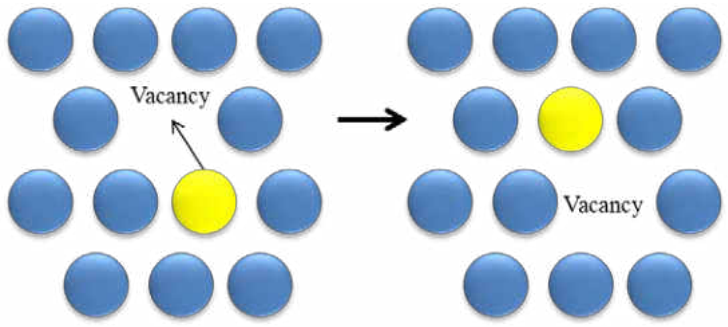

Figure 3: Schematic of the vacancy mechanism of diffusion in substitutional solutions.

The vacancy mechanism is responsible for the self-diffusion of pure metals as well as mostly all substitutional solutes in alloy systems. The Kirkendall effect is a confirmation of the vacancy mechanism of diffusion. The Kirkendall effect was shown by the experiments of Smigelskas and Kirkendall (Kirkendall, 1947) studying the diffusion of copper and zinc within the alpha-brass composition range. For simplicity, the effect will be described using a diffusion couple consisting of pure metals, A and B. In Figure 4, a diffusion couple of pure metal A and pure metal B is assembled with inert markers (i.e., refractory wires or oxide particles) placed at the interface of contact between the two end members. These markers serve as a plane of reference (lattice-fixed) from which the diffusion process can be observed in relation to the laboratory fixed frame of reference (i.e., the ends of the diffusion couple). After assembly, the diffusion couple is annealed at an elevated temperature for a considerable time and then cooled to room temperature. The diffusion couple is then sectioned perpendicular to the plane of the markers and the composition of each section is analyzed and plotted versus distance to give a concentration profile. The concentration profile reveals there has been a

migration of B atoms into the A side of the couple as well as a migration of A atoms into the B side of the couple. This result was not unknown when Smigelskas and Kirkendall performed their experiments; however, what was interesting was showing the inert markers placed in the diffusion couple had moved.

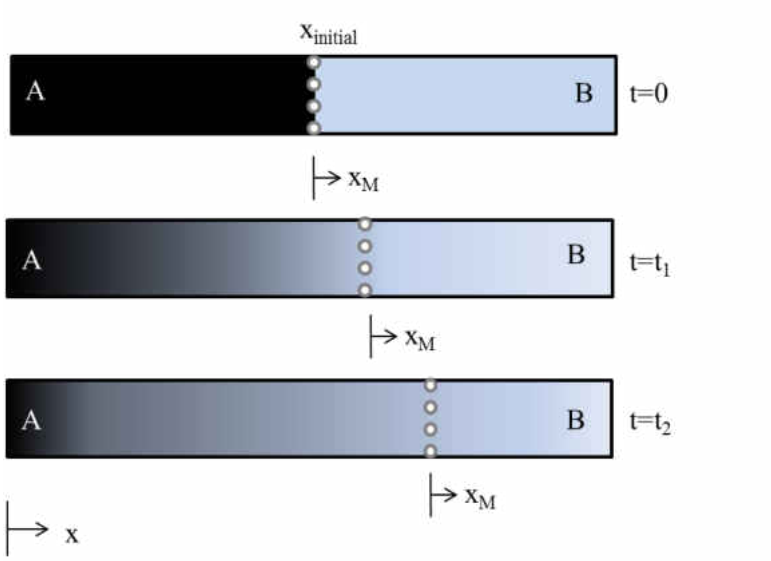

Figure 4: Schematic representations of a diffusion couple between elements A and B and a demonstration of the Kirkendall effect. Inert markers (white spots) placed at the initial interface before annealing are shifted with increasing annealing time ($t_2>t_1$) to the right (from $x_{initial}$) as the diffusion of the species B is faster than A.

The movement of the markers can be explained by maintaining that each species of atoms moves at a different rate in the system, mainly, each element has its own *intrinsic diffusivity* in the system. Figure 5 shows a schematic of the flux of A atoms, B atoms and vacancies, with species B having the faster rate of diffusion. Every time an atom

jumps, a corresponding vacancy moves, enabling a flow of vacancies in the opposite direction of the faster moving species. This side of the diffusion couple loses more atoms than it gains from the other diffusing species, resulting in shrinkage on the faster diffusing species side and swelling on the slower diffusing species side. It is possible, under these conditions, to form pores in the side of the faster moving species largely due to the stresses associated with the shrinking in the faster moving species side of the diffusion couple.

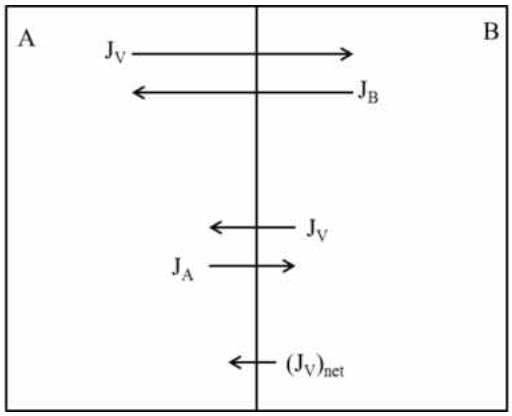

Figure 5: Schematic of the intrinsic fluxes of atoms A and B and flux of vacancies in a diffusion couple where the diffusion of B atoms is faster.

2.3 Types of Diffusion

2.3.1 Self-diffusion in metals

Self-diffusion is the diffusion of a material's atoms within itself, for example, self-diffusion in a metallic element *A* is the movement of *A* atoms within that solid. Self-diffusion is the most fundamental, and consequently one of the most studied, types of diffusion. Experimentally, self-diffusion is usually observed via the *tracer method*, where tagged atoms are used as the diffusant. These tagged atoms are either stable or radioactive isotopes that are chemically identical to the matrix material and only differ slightly in atomic mass. The effects of this difference in atomic mass between the tagged isotope and the host atom during self-diffusion can typically be neglected. In some cases, the difference in diffusion behavior due to the mass difference is of interest and can be studied. This effect is known as the isotope or mass effect and can sometimes reveal insight into the diffusion mechanism. The vacancy mechanism of diffusion, described in Chapter 2.2, is responsible for the self-diffusion of practically all metals. Figure 6(a) shows schematically a typical self-diffusion experiment for a metallic element using a tracer, A^*, of the matrix material A.

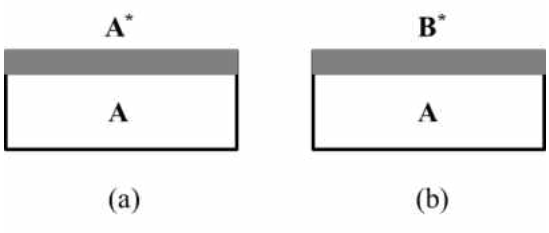

Figure 6: Schematic illustration of the initial configurations of typical thin film tracer diffusion experiments for (a) the self-diffusion of A* in A and, (b) the impurity diffusion of B* in A.

2.3.2 Tracer and impurity diffusion in metals

As described above, tracer diffusion involves tagged atoms migrating through a solid. In the case of self-diffusion, these atoms are chemically identical to the matrix, however, they can also be chemically different than the matrix. The latter case is considered *impurity* diffusion. In a typical tracer or impurity diffusion experiment, a thin film of a stable or radioactive isotope of element B^* is deposited on the matrix element A, as shown in Figure 6(b). At an elevated temperature this thin film of tagged impurity atoms diffuses through the matrix and can be measured by sectioning techniques or by depth profiling techniques, such as secondary ion mass spectrometry. The *tracer diffusion coefficient* is essentially independent of the tracer concentration and implies that the diffusion of tracer atoms in a matrix is not influenced by the presence of other tracer atoms. The tracer concentration gradient can be kept small enough that the total composition of the sample during the experiment does not change. Tracer and impurity diffusion experiments are used to study self-diffusion and impurity or solute diffusion in very dilute conditions.

2.3.3 Interdiffusion and intrinsic diffusion in metals

Interdiffusion, also referred to as chemical diffusion, occurs under a chemical potential gradient that drives the system to intermix. An example of this would be a binary diffusion couple between two pure metals, A and B. In a binary system, there is one interdiffusion coefficient to describe the interdiffusion between A and B, and it is usually concentration and temperature-dependent. Method's on how to obtain the interdiffusion coefficient will be discussed in the next chapter.

Intrinsic diffusivity is the rate of diffusivity of each element, A and B, in the binary system. In order to obtain the intrinsic diffusion coefficients, knowledge of the interdiffusion coefficient, and the location of the Kirkendall marker plane in relation to the laboratory fixed plane (or the Kirkendall plane velocity) are necessary by the use of the Darken or Darken-Manning equations described in Chapter 2.4.2.

2.4 Diffusion equations

2.4.1 Fick's Laws

There are two basic approaches to studying solid state diffusion, the *atomistic approach* and the *continuum approach*. In the atomistic approach, the diffusion behavior in a material is considered at the atomic level. The continuum approach treats the diffusion in a solid as a continuous medium, neglecting diffusion behavior at the atomic level. The

continuum approach can be used to analyze and predict micro- and macroscopic physical and chemical changes. In this study, the continuum approach was utilized for diffusion analysis.

In a single-phase, inhomogeneous alloy, atoms will migrate to decrease the concentration gradients when annealed. The diffusion flux, or number of atoms migrating through a unit area per unit time, can be obtained by taking the flux perpendicular to a given cross-sectional area to be proportional to the concentration gradient across that area. For the concentration gradient of a component *i* in one direction (x), the flux, J_i (mol/m^2-s) is given by Fick's first law (Fick, 1855)

$$\mathrm{J_i} = -\mathrm{D}\left[\frac{\partial \mathrm{C_i}}{\partial \mathrm{x}}\right] \tag{3}$$

where the proportionality constant, D (m^2/s), is called the diffusion coefficient, C_i (mol/m^3) is the concentration and x (m) is the position. Fick's first law is most convenient to use under steady state conditions, meaning, the concentration at a point does not change with time. However, if the concentration does vary with time, t (s), Fick's first law, Eq. (3), should be combined with the law of mass conservation to obtain the partial differential equation

$$\frac{\partial C}{\partial t} = -\frac{\partial J_i}{\partial x} = \frac{\partial}{\partial x}\left(D\frac{\partial C}{\partial x}\right) \tag{4}$$

When the diffusivity, *D*, is a constant (i.e., independent of concentration), Eq. (4) simplifies to a linear second-order partial differential equation of the form

$$\frac{\partial C}{\partial t} = D\frac{\partial^2 C}{\partial x^2} \tag{5}$$

In this form, the concentration as a function of position (i.e., in the x-direction) and time, C(x,t), can be approximated using Gaussian or error function solutions if the initial and boundary conditions are known. This is the case for tracer diffusivity in a chemically homogeneous system and for diffusion in ideal solid solutions. The reader is referred to the book written by J. Crank (Crank, 1975) for a more comprehensive treatment of mathematical solutions to Fick's second law and diffusion behavior.

To specify interdiffusion, the diffusion coefficient is usually denoted as $\widetilde{D}$. In solids, interdiffusion is typically a function of composition and temperature, making Eq. (4) a nonlinear differential equation. Normally, solutions for the equation in this form cannot

be obtained analytically. The determination of the interdiffusion coefficient as a function of concentration, $\widetilde{D}(C)$, can be obtained by a graphical method such as the Boltzmann-Matano analysis (Boltzmann, 1894) (Matano, 1933). Since this method was employed for the interdiffusion study in this document, elaboration of this method is provided.

Boltzmann (Boltzmann, 1894) showed that the nonlinear partial differential equation form of Fick's law can be transformed into a nonlinear ordinary differential equation when the interdiffusion coefficient is a function of concentration only by using a scaling parameter, $\lambda = x/\sqrt{t}$, where x and t represent distance and time, respectively. Using this parameter in Eq. (4) yields

$$\frac{-\lambda}{2}\frac{dC}{d\lambda} = \frac{d}{d\lambda}\left(\widetilde{D}\,\frac{dC}{d\lambda}\right) \tag{6}$$

Utilizing this transformation, Matano, considering a binary diffusion couple, applied the initial and boundary conditions $C=C_L$ for ($x<0$, $t=0$) and $C=C_R$ for ($x>0$, $t=0$) and obtained a solution in the form of

$$\widetilde{D}(C) = -\frac{1}{2}\frac{d\lambda}{dC}\int_0^C \lambda\, dC \quad \text{with the condition } \int_{C_L}^{C_R} \lambda\, dC = 0 \tag{7}$$

If the annealing time, *t*, is constant, Eq. (7) becomes

$$\widetilde{\mathrm{D}}(\mathrm{C}) = \frac{1}{2\mathrm{t}}\frac{\mathrm{dx}}{\mathrm{dC}}\int_{\mathrm{C_L}}^{\mathrm{C}} \mathrm{x}\,\mathrm{dC} \quad \text{with the condition } \int_{\mathrm{C_L}}^{\mathrm{C_R}} \mathrm{x}\,\mathrm{dC} = 0 \tag{8}$$

Satisfying the condition given gives the position of the *Matano plane,* x_o, which is required for analysis. The location of the Matano plane can be found from the experimental concentration profile. The Boltzmann-Matano method is shown schematically in Figure 7. The location of the Matano plane occurs when the areas above and below the concentration profile are equal; area A=area B, both shown in grey in Figure 7. To determine the concentration-dependent interdiffusion coefficient at a concentration, *C**, the integral $\int_{\mathrm{C_L}}^{\mathrm{C}^*} \mathrm{x}\,\mathrm{dC}$ is evaluated to obtain the area, *A**, shown in the hatched region of Figure 7. Then, the concentration gradient (or slope of the concentration profile), $m=(dC/dx)_{C^*}$, is found at the corresponding position, *x**. Finally, the interdiffusion coefficient for *C=C** is found as: $\widetilde{D}(C^*) = -A^*/(2tm)$,where t is the time. This method is valid for an infinite system, requiring the concentrations at the boundaries of the system to remain unchanged. Another requirement of this method is the volume of the diffusion couple remains constant during the diffusion process; the total molar volume, V_m, of the binary system follows Vegard's rule. Vegard's rule, $V_m = V_A N_A + V_B N_B$, is characterized by the partial molar volumes (V_A, V_B) of both components in a binary A-B system vary linearly with composition (N_A, N_B). If a system

deviates from Vegard's rule, other graphical methods such as the one derived by Sauer and Freise (Sauer & Freise, 1962) should be employed to find the concentration-dependent interdiffusion coefficients.

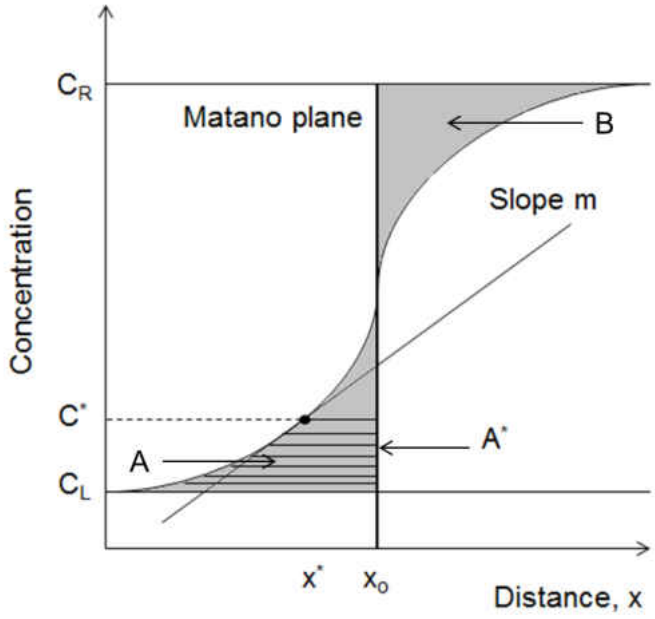

Figure 7: Schematic representation of the Boltzmann-Matano method for a binary A-B diffusion couple with starting compositions of C_L and C_R.

2.4.2 The Darken equations

The Boltzmann-Matano analysis allows for the determination of the interdiffusion coefficient as a function of concentration,$\widetilde{D}(C)$, which is essentially an average diffusion coefficient for both diffusing species in a binary system. It does not, however, give insight into the diffusion of each species, i.e., their intrinsic diffusivities. As described in

Chapter 2.2, the Kirkendall effect is proof that each diffusing species migrates at a different rate, described by the intrinsic diffusion coefficient. Darken (Darken, 1948) gave a theoretical description relating interdiffusion and intrinsic diffusion in a binary system. To explain Darken's analysis, consider a binary A-B diffusion couple (i.e., Figure 4). Inert markers are placed between the initial bonding surfaces and the diffusion couple is annealed at an elevated temperature for interdiffusion to occur. The markers become trapped at a certain composition during diffusion and move with this composition as the process continues with time. The intrinsic flux, J_i, at the marker plane, x_M, is given by

$$\mathrm{J_i} = -\mathrm{D_i}\left(\frac{\partial \mathrm{C_i}}{\partial \mathrm{x_M}}\right) \quad (i\text{=A, B}) \tag{9}$$

where D_i is the intrinsic diffusion coefficient for species i and $\partial C_i/\partial x_M$ is the concentration gradient at the maker plane. The marker plane moves in reference to the lattice frame of reference, however, it can be shown to move parabolically in time with respect to the laboratory frame of reference, i.e., $x_M = K\sqrt{t}$, where K is a constant depending upon temperature. The velocity of the Kirkendall plane is given by $\mathrm{v_K} = \mathrm{x_M}/2\mathrm{t}$. The Kirkendall velocity can also be expressed in terms of intrinsic fluxes and partial molar volumes as

$$v_K = -(V_A J_A + V_B J_B) \tag{10}$$

Given that $dC_A = -(V_B/V_A)dC_B$, Eq. (10) can be written as

$$v_K = V_B(D_B - D_A)\frac{\partial C_B}{\partial x_M} \tag{11}$$

where $\partial C_B/\partial x_M$ is the concentration gradient at the Kirkendall marker plane. Following Darken's analysis, the interdiffusion flux at the Kirkendall plane is expressed as

$$\tilde{J} = -D_i\frac{\partial C_i}{\partial x_M} \pm v_K C_i \text{ (i=A,B)} \tag{12}$$

where the first term on the right-hand side of the equation is the sum of the intrinsic diffusion flux of one of the components, *i*, and the $v_K C_i$ term represents the Kirkendall drift. Combining Eq. (11) and Eq. (12), a general expression for the interdiffusion coefficient can be obtained as

$$\tilde{D} = C_A V_A D_A + C_B V_B D_B \tag{13}$$

When the partial molar volumes are equal and do not change with composition ($V_m=V_A=V_B$), Eq. (13) can be written as

$$\widetilde{D} = N_A D_A + N_B D_B \tag{14}$$

where N_A and N_B are the mole fractions of components A and B, respectively. Eq. (14) is known as Darken's equation, and in conjunction with Eq. (11), it can be used to determine the intrinsic diffusion coefficients of A and B from the interdiffusion coefficient.

As mentioned, the actual driving force for diffusion is a chemical potential gradient, $\partial\mu_i/\partial x$, not the concentration gradient, $\partial C_i/\partial x$ as assumed in Fick's laws. In terms of the chemical potential gradient of component *i*, the intrinsic flux in a binary system can be written as

$$J_i = -\beta_i C_i \frac{\partial \mu_i}{\partial x} \quad (i\text{=A,B}) \tag{15}$$

where β_i is the atomic mobility and μ_i is the chemical potential of component *i*. Chemical potential can be described by the equation

$$\mu_i = \mu_i^o + RT \ln a_i \quad (i\text{=A,B}) \tag{16}$$

where $\mu_i^o$is the standard chemical potential at 1 atm and 298K, *R* is the ideal gas constant (8.314 J/mol-K) and a_i is the thermodynamic activity of component *i*. Thermodynamic activity is given by $a_i = \gamma_i N_i$, where γ_i is the activity coefficient. The activity is related to the thermodynamic factor, Φ, by $\partial \ln a_i / \partial \ln N_i$ (Philibert, 1991). The intrinsic diffusion coefficient and the tracer diffusion coefficient, D_i^*, of species *i* can be related by combining Eq. (15), the Nernst-Einstein relation; $D_i^* = \beta_i RT$ and substituting into Eq. (9) to yield (Darken, 1948)

$$D_i = \beta_i RT\Phi = D_i^*\Phi \quad (i\text{=A,B}) \tag{17}$$

Finally, an expression for interdiffusion in terms of the thermodynamic factor and tracer diffusivities for the binary A-B system is given by (Darken, 1948)

$$\widetilde{D} = (N_A D_B^* + N_B D_A^*)\Phi \tag{18}$$

Eq. (17) and Eq. (18) are Darken's equations used in diffusion analysis for substitutional binary alloys. It should be noted that for an ideal solid solution the activity coefficient is $\gamma_i=1$ and activity, $a_i=N_i$, therefore, the thermodynamic factor, $\Phi=1$ (Raoult's law) (Philibert, 1991). However, Φ deviates from unity for non-ideal solutions. Larger deviations, and therefore larger thermodynamic factors, are often observed for intermetallic compounds due to the attractive interaction between phase constituents, especially in ordered compounds. It should be noted that Eq. (18) does not account for the flux of vacancies present during the interdiffusion process required for the Kirkendall effect to occur. A correction term, *S*, multiplied by the right-hand side of Eq. (18), was introduced by Manning and is a culmination of the tracer diffusion coefficients and correlation factors of the system components. This correction term is known as the *total vacancy wind factor* or *Manning factor*. For a further explanation of vacancy wind effects, the reader is referred to the works of J.R. Manning (Manning J. R., 1968) (Manning J. , 1967).

As mentioned above, diffusion processes can be a function of concentration *and* temperature. Frequently, the temperature dependence of diffusion can be described by the Arrhenius relation

$$\mathrm{D} = \mathrm{D_o}\exp\left(\frac{-\mathrm{Q}}{\mathrm{RT}}\right) \tag{19}$$

presented here in general form since the interdiffusion coefficient, $\widetilde{D}$, intrinsic diffusion coefficient, D_i, and the tracer diffusion coefficient, D_i^*, can all exhibit this temperature dependence. D_o is the *pre-exponential* or *frequency factor* and has the same units as the diffusion coefficient (m^2/s). *Q* is the *activation energy* for the diffusion process, typically given in kJ/mole. *R* is the ideal gas constant and *T* is the temperature in Kelvin. From a semi-logarithmic plot of the diffusion coefficient versus the quantity 1/T (1/temperature), the activation energy can be calculated from the slope as shown schematically in Figure 8.

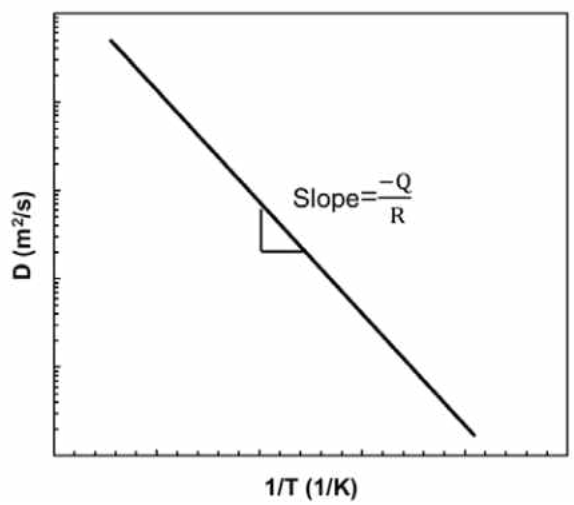

Figure 8: Schematic illustration of the determination of the activation energy for diffusion.

2.5 Magnesium and diffusion

2.5.1 Magnesium and magnesium alloys

Magnesium (Mg) is the lightest weight metal available for structural applications. Current use of Mg in the electronics, military and transportation industries is greatly increasing due to the unique properties and advantages afforded by these alloy systems and is forecasted to continue increasing (Mordike & Ebert, 2001) (Urbance, Field, Kirchain, Roth, & Clark, 2002) (Cho, et al., 2009) (Bamberger & Dehm, 2008). The density of Mg is 1.74 g/cm^3, making it 1/5th that of iron, 2/5th that of titanium and 2/3rd that of aluminum (Avedesian & Baker, 1999). Magnesium alloys also exhibit good damping capacity, excellent castability, weldability and machinability (Mordike & Ebert, 2001). They have been used in myriad applications such as cell phone and laptop cases, automobile instrument panels, steering wheels and even internal engine components and helicopter gearboxes, etc (Mordike & Ebert, 2001) (Cho, et al., 2009). There have been improvements in the corrosion resistance of Mg alloys with the use of high purity Mg and improvements in the creep resistance with additions of rare earth elements such as yttrium and neodymium. Misconceptions with regards to the flammability of Mg alloys are often encountered when in fact, in solid form, Mg is very difficult to ignite. Only in powder or machine chip form is it necessary to take precautions against flammability issues. Continued efforts to develop new Mg alloys or modify current ones for further improved corrosion resistance, creep resistance, ductility and strength are ongoing (Bamberger & Dehm, 2008).

Magnesium is the eighth most common element in the world and the sixth most abundant metal. The main sources are seawater, containing about 0.14% Mg and minerals such as Carnallite ($KMgCl_36(H_2O)$), Dolomite ($MgCO_3CaCO_3$) and Magnesite ($MgCO_3$). There are three main extraction processes to obtain Mg metal; Calcination, the Pidgeon process, and the Dow process. Calcination involves heating Magnesite to produce Magnesium Oxide, MgO which is then mixed with petroleum coke heated to separate the oxygen from the magnesium. The Pidgeon process, or thermal reduction method, involves the calcination of Dolomite to produce MgO and CaO. The MgO is then combined with powdered ferrosilicon and charged in a retort and heated under vacuum at approximately 1473K (1200°C) to produce Mg vapor. The Mg vapor is then condensed to crystals. The Dow process is the electrolysis of Mg. Seawater and Dolomite are precipitated as magnesium hydroxide, $Mg(OH)_2$ and subsequently treated with HCl to yield magnesium chloride, $MgCl_2$. The magnesium chloride is then placed into an electrolysis cell to reduce it to Mg and Cl. There are also efforts to promote and increase the Mg recycling industry which is increasingly attractive considering the positive impact on the environment (Zaludova, 2005).

Magnesium has a hexagonal close packed (HCP) crystal structure with a lattice parameter a=0.320 nm and a c/a ratio of 1.624. Figure 9 is a schematic of the Mg unit cell.

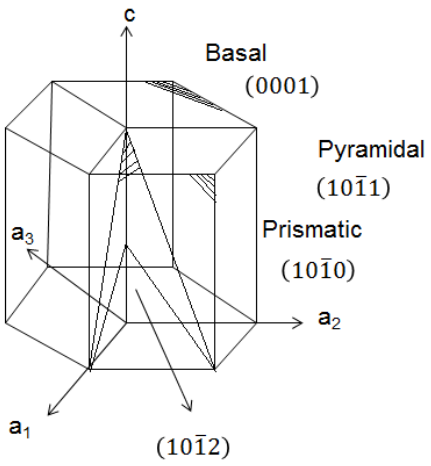

Figure 9: Schematic of a hexagonal clos-packed (HCP) unit cell.

Mg has a relatively low melting temperature of 923K (650°C), and consequently Mg alloys have relatively low melting temperatures as well. Mg alloys have limited room temperature workability due to the limited number of slip systems available in the HCP unit cell (Avedesian & Baker, 1999). Primary dislocation slip occurs on the basal (0001) plane in the $\langle 11\bar{2}0 \rangle$ close packed direction. Secondary slip occurs on the prismatic $\{10\bar{1}0\}$ planes in the $\langle 11\bar{2}0 \rangle$ direction. Deformation is accommodated by the formation of twins at higher strain rates due to the lack of sufficient slip systems at lower strain rates and ambient temperature. At elevated temperatures, dislocation slip can also occur on the pyramidal $\{10\bar{1}1\}$ planes in the $\langle 11\bar{2}0 \rangle$ direction. For this reason, Mg alloys are normally hot worked at temperatures above 473K (200°C) (Dow Chemical Company, 1982).

The most commonly used Mg alloys are currently based on the Mg-Al system with the AZ and AM series of alloys. The Mg alloy designation scheme is presented in two parts, the two main alloying elements as two letters and their relative weight percentages with the element present in the highest amount first. Temper designations for Mg alloys are similar to those used for Al alloys. Some common commercial Mg alloying component designations are shown in Table 1. Following this scheme for example, the widely used AZ91 alloy consists of a nominal 9 wt.% aluminum and 1 wt.% zinc. Occasionally a letter, A through E, is presented at the end of the alloy designation; this represents the purity modification. D and E represent higher purity Mg used in the alloying process and is typically used for improved corrosion resistance.

Table 1: Mg alloy letter designations for some common alloying elements

Letter	Representative Element
A	Aluminum
Z	Zinc
M	Manganese
K	Zirconium
W	Yttrium
E	Rare earths (Nd, Gd, Dy, etc,)
Q	Silver

As mentioned above, the AZ (Aluminum-Zinc) and AM (Aluminum-Manganese) Mg alloy series are the most commonly used Mg alloys. Some common commercial cast and wrought Mg alloys are presented in Table 2 with some of their corresponding fabrication processes and applications.

Table 2: Some common Mg alloys and their manufacturing processes and applications

Cast alloys	
Alloy	Application
AM60A/B	High-pressure die-casting, excellent ductility in the –F (as Fabricated) condition Uses: fans and automobile wheels
AZ91C/E	General purpose, sand and permanent mold-casting Uses: aircraft parts, gearboxes, machinery components
AZ91B/D	General purpose die-casting Uses: computer parts, automobile parts, sporting goods, household appliances, cameras
Wrought Alloys	
AZ31B/C	General purpose, moderate strength alloy
ZK60A	Higher strength alloy Uses: batteries, military components, sporting equipment
WE43	Improved high temperature properties and corrosion resistance Uses: military applications

Since Mg alloys are mostly worked at elevated temperatures, diffusion of the alloy constituents plays a major role in the resulting microstructure and properties. Many Mg alloys are age-hardenable and are available in the –T5 (artificially aged), or –T6 (solutionized then artificially aged) temper conditions. These secondary processes involve diffusion of the solute elements to form precipitates that can increase the strength and in some cases, the creep resistance of the alloys. For precipitation-hardening to occur successfully, the solute addition needs to have a significant solubility range in Mg at higher temperatures that drops quickly with decreasing temperature. Therefore, both primary and secondary processing is critical in determining many resulting properties.

2.5.2 Diffusion in magnesium

Mg and its natural compounds are widely studied due to their abundance in mineral form within the earth's crust. Diffusion processes and behavior are important in geological studies as well. Due to this, most of the available diffusion literature with respect to Mg compounds is of a geological nature. However, since this investigation is geared towards metallurgical aspects, a review of the available diffusion literature for Mg in its metallic form only will be presented. In comparison to some other common metallic elements used in commercial alloys such as iron and nickel, magnesium is used less frequently for engineering and structural applications. Due to this, fundamental research, including diffusion research, is somewhat limited for Mg based systems. The available self-diffusion, some relevant tracer and impurity diffusion, as well as other relevant diffusion experiments will be discussed.

The self-diffusion of magnesium has been studied experimentally by Shewmon and Rhines in 99.9% pure polycrystalline Mg (Shewmon & Rhines, Rate of Self-Diffusion in Polycrystalline Magnesium, 1954), and in 99.9% pure single crystal Mg by Shewmon (Shewmon, 1956) with the radioisotope ^{28}Mg from 741 to 900K (468 to 627°C). Combronde and Brebec also studied self-diffusion in 99.99% pure single crystal Mg with the same radioisotope in the temperature range of 773 to 903K (500 to 630°C) (Combronde & Brebec, Anisotropie d'autodiffusion du magnesium, 1971). A first principles based study of the self-diffusion in Mg was completed by Ganeshan *et al.*

(Ganeshan, Hector Jr., & Liu, 2010). Table 3 presents a summary of diffusion parameters reported from these studies. Figure 10 shows a comparison of the temperature dependence of Mg self-diffusion from these studies. As seen in Figure 10 and Table 3, the experimental results of Shewmon and Combronde and Brebec agree very well, reporting similar pre-exponential factors and activation energies for self-diffusion. The first principles based model of self-diffusion in Mg from Ganeshan *et al.* is slightly lower in magnitude as well as activation energy than the experimental results. Also, from Figure 10, it is evident that the anisotropy for diffusion (i.e. different diffusion rate depending on the direction of the HCP crystal) is quite small.

Table 3: Summary of self-diffusion parameters, pre-exponential factor, D_o, and activation energy, Q, in magnesium

D_o (10^{-4} m^2/s)	Q (kJ/mol)	Temperature range (K)	Method	Investigator (Year)
1.0	134	741-900	^{28}Mg, 99.9% Mg, polycrystalline, mechanical sectioning	Shewmon and Rhines (Shewmon & Rhines, Rate of Self-Diffusion in Polycrystalline Magnesium, 1954) (1954)
1.0 (|| c axis)	135	741-908	^{28}Mg, 99.9% Mg, single crystals, mechanical sectioning	Shewmon (Shewmon, 1956) (1956)
1.5 (⊥ c axis)	136			
1.78 (|| c axis)	139	775-906	^{28}Mg, 99.99% Mg, single crystals, mechanical sectioning and residual activity	Combronde and Brebec (Combronde & Brebec, Anisotropie d'autodiffusion du magnesium, 1971) (1971)
1.75 (⊥ c axis)	138			
$4.9x10^{-2}$ (|| c axis)	121	300-900	Modeled first principles	Ganeshan *et al.* (Ganeshan, Hector Jr., & Liu, 2010) (2010)
$4.5x10^{-2}$ (⊥ c axis)	119			

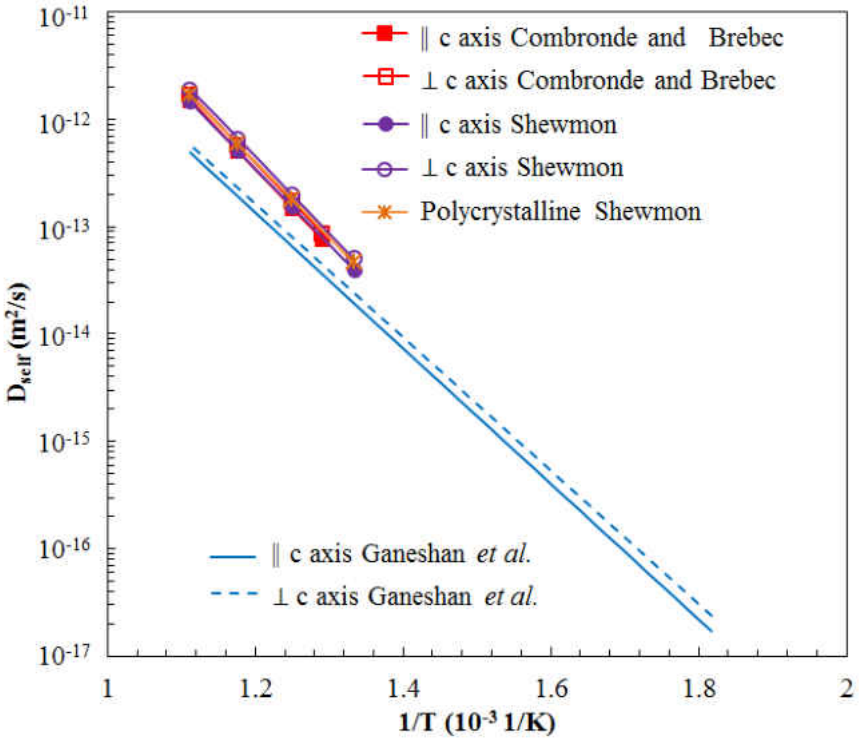

Figure 10: Comparison of the self-diffusion coefficient in magnesium.

Table 4 presents a summary of some of the available impurity diffusion studies in polycrystalline Mg. Figure 11 is a comparison of some available impurity diffusion studies in Mg as well as Mg self-diffusion. All of these studies were conducted using radioactive isotopes of the impurity elements in at least 99.8% pure polycrystalline Mg and utilizing either the serial sectioning or residual activity method. As seen in Figure 11, the range of impurity diffusivities spans several orders of magnitude. For some of these impurity elements, diffusion data in Mg single crystals has also been reported, typically by the same investigators. For a more complete compilation of the available

impurity and self-diffusion data in Mg, the reader is referred to the review article by S. Fujikawa (Fujikawa S. , 1992).

Table 4: Diffusion parameters for several impurities in polycrystalline magnesium

Element	D_o (10^{-4} m^2/s)	Q (kJ/mol)	Temperature range (K)	Method	Investigator (Year)
Mn	0.76	154	843-903	^{54}Mn, 99.9% Mg, residual acivitiy	Fujikawa (Fujikawa S. , 1992) (1992)
Zn	0.41	120	740-893	^{65}Zn, 99.8% Mg, serial sectioning	Lal (Lal, 1967) (1967)
Ag	0.34	119	749-794	^{110m}Ag, 99.8% Mg, serial sectioning	Lal (Lal, 1967) (1967)
Fe	$4x10^{-6}$	88.8	673-873	^{59}Fe, 99.9% Mg, residual activity	Pavlinov (Pavlinov, Gladyshev, & Bikov, 1968) (1968)
Ni	$1.2x10^{-5}$	95.9	673-873	^{63}Ni, 99.9% Mg, surface decrease method	Pavlinov (Pavlinov, Gladyshev, & Bikov, 1968) (1968)
In	$5.2x10^{-2}$	119	745-883	^{114}In, 99.8% Mg, serial sectioning	Lal (Lal, 1967) (1967)
U	$1.6x10^{-5}$	115	773-893	^{235}U, 99.9% Mg, residual activity	Pavlinov (Pavlinov, Gladyshev, & Bikov, 1968) (1968)

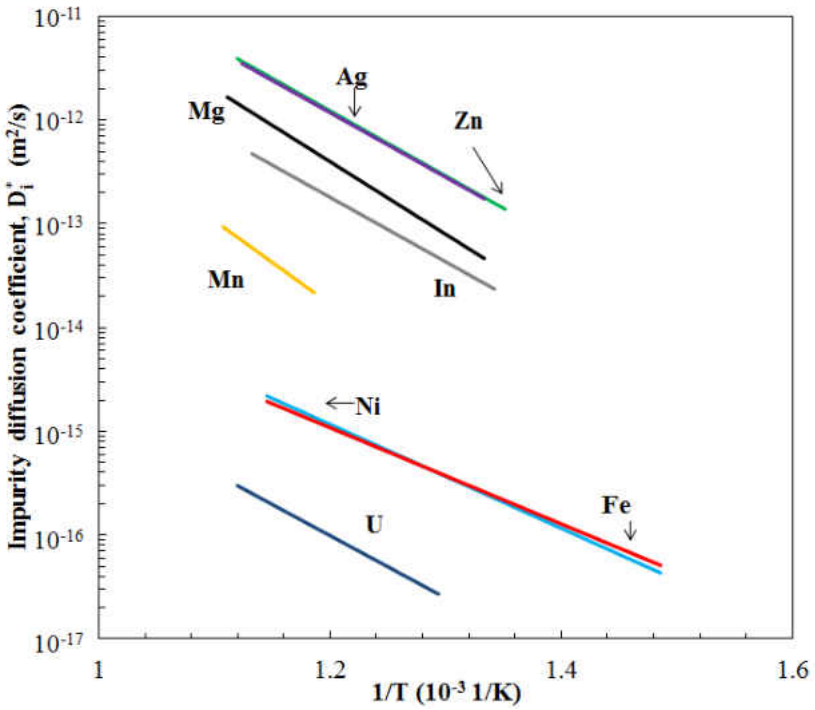

Figure 11: Comparison of the impurity diffusivities of Ag, Fe, In, Mn, Ni, U and Zn and self-diffusion in polycrystalline magnesium.

Tracer diffusion studies are more widely available in the literature due to their fundamental nature and well established experimental procedure and analytical evaluation. Interdiffusion studies, however, are also commonly conducted. Typically, diffusion couples are used to study intermetallic phase formation and growth as well as interdiffusion parameters. Diffusion couples can be used to verify the phase formations, compositions and temperatures of equilibrium phase diagrams. Diffusion couples are still being utilized to experimentally determine and/or verify equilibrium phase diagrams for several Mg binary systems including, Mg-Al, Mg-Y, Mg-RE (RE=Nd, Pr, Dy, Ce)

(Brubaker & Liu, 2004) (Tanguep Njiokep, Salomon, & Mehrer, 2001) (Funamizu & Watanabe, 1972) (Zhao, Qin, Ren, Pei, Chen, & Guo, 2010) (Xu, Chumbley, Weigelt, & Laabs, 2001). Rare earths (RE's) are of prominent interest due to their added strength and creep resistance in Mg alloys such as WE43.

The Mg binary system of interest in this study is the Mg-Al system. The Mg-Al binary system is the most common in commercial Mg alloys and is also common in some commercial Al alloys as well. The equilibrium phase diagram for the Mg-Al system is given in Figure 12 (Okamoto, 1998). There are several intermetallic phases present, namely, β-Mg_2Al_3, ε-$Al_{30}Mg_{23}$, γ-$Al_{12}Mg_{17}$, and the high temperature λ phase. Some significant solid solubility is exhibited for both elements, more so for Mg in Al than for Al in Mg. The melting temperatures of Mg (923K) and Al (933K), are very similar. In heat treatable Mg-Al based alloys, precipitates of the γ-$Mg_{17}Al_{12}$ phase develop and give added strength.

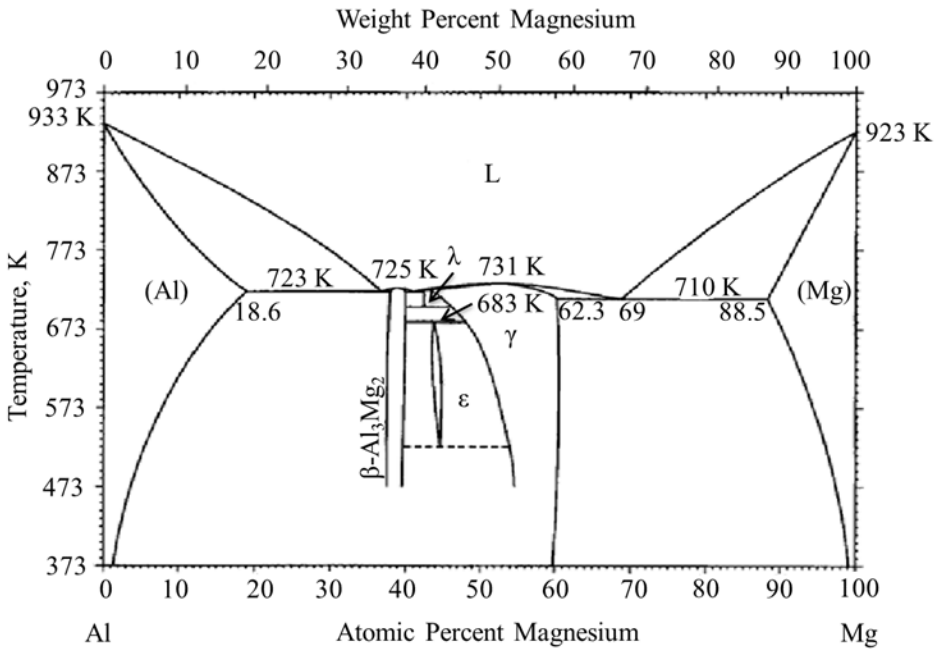

Figure 12: Equilibrium phase diagram for Mg-Al (Okamoto, 1998).

The growth of intermetallic phases in the Mg-Al system was investigated via diffusion couples by Brubaker and Liu (Brubaker & Liu, 2004) and Tanguep Njokep *et al.* (Tanguep Njiokep, Salomon, & Mehrer, 2001). Brubaker and Liu studied the growth of intermetallic phases in the Mg-Al system in the temperature range of 633 to 693K (360 to 420°C). In the diffusion couples annealed at temperatures between 648K and 693K, only the β-Mg_2Al_3 and γ-$Mg_{17}Al_{12}$ phases were observed. In the diffusion couples annealed at 633K and 640K, the β-Mg_2Al_3, γ-$Mg_{17}Al_{12}$ and ε-$Al_{30}Mg_{23}$ phases were observed. The β-phase was observed to grow much thicker and have higher growth constants than both the γ and ε phases when present. In the growth study conducted by Tanguep Njokep *et al.,* the parabolic growth rate dependence was verified for both the β

and γ phases in the temperature range of 604 to 709K (331 to 436°C). The occurrence of the ε-phase was not confirmed qualitatively in any of the diffusion couples studied. Again, it was reported that the β-phase developed a thicker layer and had higher parabolic growth constants than the γ-phase.

A review of diffusion data for this binary system reveals little reliable data. The first available calculation of interdiffusion parameters for the Mg-Al system was reported by Heumann and Kottmann (Heumann & Kottmann, 1953) in which experimental results from Bungardt (Bungardt, 1937) were utilized. Heumann and Kottmann reported interdiffusion coefficients for the intermetallic phases, β-Mg_2Al_3 and γ-$Mg_{17}Al_{12}$, and did not report the observance of the ε-$Al_{30}Mg_{23}$. Heumann and Kottmann reported that the initial interface of the diffusion couple moved toward the magnesium side and was situated in the γ-$Mg_{17}Al_{12}$ phase. From this they calculated intrinsic diffusion coefficients for Al and Mg in the γ-$Mg_{17}Al_{12}$ at that plane and concluded that Mg diffused more rapidly than Al. All subsequent interdiffusion investigation in this binary system suggest opposite conclusions to those provided by Heumann and Kottmann. Funamizu and Watanabe (Funamizu & Watanabe, 1972) investigated the interdiffusion between Mg and Al in the temperature range of 598 to 698K (325 to 425°CK). Multiple diffusion couples were utilized to measure the growth kinetics of the intermetallic phases that formed. Funamizu and Watanabe reported the presence of the β- Mg_2Al_3 and γ-$Mg_{17}Al_{12}$ intermetallic phases only, noting that the ε-$Al_{30}Mg_{23}$ phase was not observed.

The growth rates for both phases were reported to follow parabolic growth behavior (Eq. 2) in the temperature range investigated. It was reported that the activation energy for growth was smaller for the β-phase than for the γ-phase. Interdiffusion coefficients were determined for both intermetallic phases using two different methods, discussed further in Chapter 5.1.3. Funamizu and Watanabe reported that interdiffusion in the β-phase was faster than in the γ-phase. In some diffusion couples, the researchers employed inert alumina (Al_2O_3) markers to study intrinsic diffusivity. The marker plane was reported to shift towards the Al side of the diffusion couple and was located in the β-phase near the Al/β interface, contrary to what Heumann and Kottman reported. Funamizu and Watanabe noted that in the original experiments conducted by Bungardt, inert markers were not used and the researchers could have mistaken some crack-like lines present in the couple as a marker plane. Funamizu and Watanabe concluded that Al intrinsically diffuses faster than Mg in the β-phase at the marker plane location. Due to the lack of consistent interdiffusion and intrinsic diffusion data, as well as the composition dependence of interdiffusion, further investigation of the diffusion behavior of the Mg-Al binary system is needed.

3 RESEARCH METHODOLOGY

3.1 Experimental procedure

3.1.1 Interdiffusion experiments

The solid-to-solid diffusion couple technique was employed to study interdiffusion between Mg and Al. Polycrystalline Mg (99.9%) and Al (99.999%) from SCI Engineered Materials, Inc.™ and Alfa Aesar®, respectively, were sectioned into discs, 10 mm in diameter and 2 mm in thickness. These polycrystalline metals typically had grain sizes ranging from 30 to 60 µm. For the assembly of diffusion couples, the disc specimens were metallographically prepared, starting with 600 grit silicon carbide (SiC) paper and finishing with a 1 µm alumina (Al_2O_3) suspension. A non-oxidizing lubricant (ethanol or oil-based) was used at each stage of preparation for both Mg and Al. Any contact with water was eliminated for the entire preparation process to minimize oxidation effects. The Mg vs. Al diffusion couples were then assembled with 2 mm-thick inert, alumina spacers in stainless steel jigs as schematically illustrated in Figure 13.

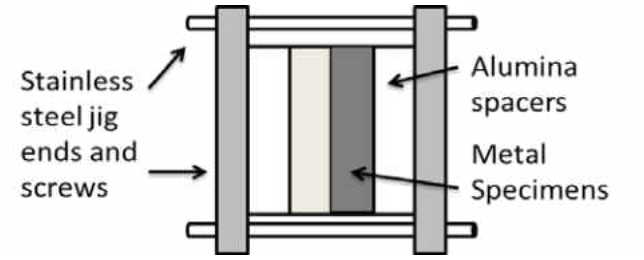

Figure 13: Schematic of the diffusion couple stainless steel jig assembly with the two disk specimens placed between inert alumina spacer disks.

The diffusion couple jig assemblies were placed in quartz capsules that were repeatedly evacuated to ~10^{-4} Pa (10^{-6} Torr) with hydrogen and ultra-high purity argon flushes between each evacuation. Before the final seal, the capsule was backfilled with a mixture of ultra-high purity argon and hydrogen (<10%) to a pressure that would be slightly greater than ~ 10^5 Pa (1 atm) at the temperature of the respective anneal. Each quartz capsule was placed in a Paragon Bluebird™ furnace, preheated to the annealing temperature. The temperature of each diffusion couple was monitored with an independent type-K thermocouple for the duration of each anneal. Three diffusion couples were assembled and annealed at 573K, 623K and 673K (300, 350, 400°C) for 720, 360, and 240 hours, respectively.

The quartz capsule was quenched in water at room temperature after the diffusion anneal. The entire diffusion couple assembly including the stainless steel jig was mounted in epoxy and cross-sectioned using a Buehler IsoMet™ saw with a low-speed

diamond wafering blade and an oil-based lubricant. The cross-sectioned specimens were then metallographically prepared, again using a non-oxidizing lubricant, for OM and SEM. Each diffusion couple was examined using OM first to check the quality of the diffusion bond, then using SEM (Hitachi™ S-3500N) equipped with XEDS to determine the constituent phases. The native oxides of Mg and Al, initially present at the surface of the disc samples, served as the marker in these diffusion couples.

Electron microprobe analysis, EPMA (JEOL™ Superprobe 733) was employed to determine the concentration profiles for each couple at 20kV, utilizing a point-to-point scan with a 5 μm step size. The pure metals, Mg (99.9%) and Al (99.999%) at the terminal ends of the couple were used as the calibration standards. A ZAF correction was employed for converting the X-ray intensity to the concentration. The concentration profiles obtained from EPMA for each phase were curve fit using piece-wise continuous polynomial functions, up to the 3rd order. The fitted concentration profiles were then used for analysis. The molar volumes of Mg, γ-$Mg_{17}Al_{12}$ (PDF# 01-073-1148), β-Mg_2Al_3 (PDF# 00-029-0048), and Al were estimated to be 14 cm^3/mol, 12.2 cm^3/mol, 11.6 cm^3/mol, and 10 cm^3/mol, respectively. A molar volume correction was applied to account for the difference in molar volume between phases, but the variation in molar volume within each phase (i.e., concentration-dependent) was assumed negligible.

3.1.2 Mg Self-diffusion

A Mg self-diffusion study was conducted using the stable isotope, ^{25}Mg in polycrystalline Mg via the tracer method. Diffusion anneals were carried out at 523, 573, 623, and 673K (250, 300, 350, 400°C) for 12, 4, 1, and 0.5 hours, respectively. Penetration profiles were obtained by depth profiling with secondary ion mass spectrometry (SIMS). These depth profiles, along with the thin film solution to the diffusion equation, were employed to extract the self-diffusion coefficients of Mg.

SIMS utilizes a primary ion beam, instead of an electron beam as in EPMA described above, that sputters layers of atoms on the specimen surface. Some of the sputter ejected atoms are ionized and filtered through a mass detector and counted as a function of time. A profilometer is used to measure the depth of the sputtered crater. A sputter rate is determined in conjunction with this measured depth and the sputtering time for the penetration profile to determine the depth. This depth profile is then used for diffusion analysis. For further details, the analysis of self-diffusion and impurity diffusion from SIMS depth profiles has been reviewed by Petuskey (Petuskey, 1983).

Magnesium occurs naturally in mainly three stable isotopes, ^{24}Mg, ^{25}Mg, and ^{26}Mg, with ^{24}Mg in the highest abundance. To accurately measure the penetration profiles of the ^{25}Mg film into the Mg substrate, isotopic ratio measurements as a function of depth are preferred rather than the absolute abundance to minimize instrument variability.

Isotopic ratios of the minor isotopes (^{25}Mg and ^{26}Mg) to the major isotope (^{24}Mg) were measured via depth profiling using a Cameca IMS 3f SIMS. An O^{2+} primary ion beam source at 10kV (5.5kV on the sample) and a 60 μm detection area were used. These isotope ratios are shown in Table 5 and were in agreement with standard reference data from NIST.

Table 5: Isotope ratios determined from SIMS depth profiling for the pure Mg substrate and ^{25}Mg enriched isotope target.

	^{25}Mg/^{24}Mg ratio (SD)	^{26}Mg/^{24}Mg ratio (SD)
Reference value	0.127	0.139
Mg substrate	0.129 (<0.001)	0.138 (<0.001)
^{25}Mg enriched target	50.8	0.139

Disk specimens, 7.5mm in diameter and 2mm thick, were prepared from a rod of 99.9% pure Mg from Alfa Aesar® as the substrates. These Mg substrates were metallographically polished starting with 600 grit SiC paper down to 0.02 μm using a colloidal silica solution. In each polishing step, a non-oxidizing lubricant, either oil or ethanol based, was utilized to minimize oxidation of the substrate. Any contact with water was eliminated during the preparation process. The Mg substrates had a grain size ranging from 30-60 μm.

The isotopic sputtering target of ^{25}Mg was obtained from Oak Ridge National Laboratory and had an enrichment percentage of 97.87% of the isotope ^{25}Mg. The Mg substrates were RF plasma etched in situ prior to deposition to remove the native oxide layer. A

thin film, approximately 100 nm in thickness, of the ^{25}Mg isotope was deposited via DC magnetron sputtering in an Ultra High Vacuum deposition system designed for highly reactive materials like Mg to ensure the film did not oxidize during deposition. The depositions were performed in ~5 mTorr of Ar (99.9999%) after a deposition chamber pressure around 10^{-8} Torr was obtained.

After deposition of the ^{25}Mg diffusant, the thin film samples were encapsulated in quartz capsules. Prior to sealing the capsules, three hydrogen and ultra-high purity argon flushes were performed in between evacuations down to ~10^{-4} Pa (10^{-6} Torr). The capsule was then evacuated to ~10^{-4} Pa and backfilled with and ultra-high purity Ar and H (<10%) mix to a pressure that would provide slightly higher than 10^{5} Pa (1 atm) at the annealing temperature. The encapsulated specimens where then placed in a preheated furnace (same as above) and annealed at the designated temperature and time. The temperature of the specimen was monitored independently with a type-K thermocouple for the annealing duration. After annealing, the capsules were quenched in water at room temperature. SIMS depth profiles were obtained using a Cameca IMS 7f from each sample using an O^{2+} ion beam, an accelerating voltage of 10 kV, a 200 μm raster area, and a 60 μm detection area. These depth profiles were then employed for further analysis to calculate the Mg self-diffusion coefficient.

3.1.3 Al impurity diffusion in Mg

The thin film technique and SIMS depth profiling were also employed to investigate the impurity diffusion of pure Al in polycrystalline, 99.9% pure Mg. Several thin film samples were annealed at 573, 623, and 673K (300, 350, 400°C) for 2, 0.5 and 0.5 hours, respectively. Secondary Ion Mass Spectrometry (SIMS) was again, employed to obtain penetration profiles. Pure Mg disk specimens, 10 mm in diameter and 2 mm in thickness, were prepared from a Mg rod from SCI Engineered Materials, Inc.^{TM}. These substrates were metallographically prepared similarly to the method above for the self-diffusion specimens.

The prepared Mg substrates were RF plasma etched in situ prior to deposition to remove the native oxide layer. An Al film approximately 500 nm thick was deposited by DC magnetron sputtering under ~4 mTorr of Ar (99.9999%) after a deposition chamber pressure of approximately $1x10^{-7}$ Torr was obtained. These thin film specimens were then encapsulated and annealed in the same manner as the self-diffusion specimens. SIMS depth profiles were obtained for the analysis of Al impurity diffusion in Mg using a Cameca IMS 3f with an O^{2+} primary ion beam source at 10 kV, a 150 μm raster area, and a 30 μm detection area.

3.2 Analytical framework

3.2.1 Intermetallic phase layer growth

For diffusion-controlled growth of a phase with a semi-infinite boundary condition, thickness of the growing phase after time t, of annealing can be described by (Philibert, 1991)

$$\mathrm{k_p} = \frac{x^2}{2\mathrm{t}} \tag{20}$$

where x is the thickness of the layer and k_p is the parabolic growth constant. Typically, the temperature dependence of the parabolic growth rate constant follows the Arrhenius relation

$$\mathrm{k_p} = \mathrm{k_o}\exp\left[\frac{-\mathrm{Q_k}}{\mathrm{RT}}\right] \tag{21}$$

where R (J/mol-K) is the ideal gas constant, Q_k is the activation energy (J/mol), and T is the annealing temperature in Kelvin. In this study, the growth of β-Mg_2Al_3 and γ-$Mg_{17}Al_{12}$ intermetallic phases are assumed to be diffusion controlled for initial analysis based on previous experimental results (Funamizu & Watanabe, 1972) (Tanguep Njiokep, Salomon, & Mehrer, 2001).

3.2.2 Interdiffusion and Intrinsic Diffusion

The Boltzmann-Matano method (Chapter 2.4.1) (Boltzmann, 1894) (Matano, 1933) was employed to determine the interdiffusion fluxes of individual components and the interdiffusion coefficients as a function of concentration. The location of the Matano plane, x_o, was found by numerical integration of the concentration profile to satisfy

$$\int_{C_i^{+\infty}}^{C_i^o} x dC_i + \int_{C_i^o}^{C_i^{-\infty}} x dC_i = 0 \quad \text{(i=Mg or Al)} \tag{22}$$

where x is the distance, C_i^o is the concentration of component i at the Matano plane, $C_i^{+\infty}$ and $C_i^{-\infty}$ are the concentrations of component i at the terminal ends. The interdiffusion flux, $\widetilde{J_i}$ for each component was calculated using the relation (Dayananda & Kim, 1979)

$$\widetilde{J_i} = \frac{1}{2t}\int_{C_i^{+\infty}}^{C_i}(x - x_o)\, dC_i \tag{23}$$

Combining Eq. (23) and Fick's first law yields the relation

$$\widetilde{D}_i = \frac{\frac{1}{2t}\int_{C_{i\pm\infty}}^{C_i}(x-x_o)dC_i}{\frac{\partial C_i}{\partial x}} \quad (i = 1,2,3,\dots,n) \tag{24}$$

Concentration-dependent interdiffusion coefficients were calculated for each phase using Eq. (24).

The integrated interdiffusion coefficient, $\widetilde{D}_{i,\Delta x}^{int}$, is a material constant given by (Dayananada, 1993) (Dayananda, 1996)

$$\widetilde{D}_{i,\Delta x}^{int} = \int_{x_1}^{x_2}\widetilde{J}_i dx \quad (i=1, 2,\dots n) \tag{25}$$

where x_2 is greater than x_1 for positive fluxes and x_2 is smaller than x_1 for negative fluxes. Integrated interdiffusion coefficients were calculated for each intermetallic phase observed. $\widetilde{D}_{i,\Delta x}^{int}$ for a material system is the same irrespective of the end member compositions. The activation energy for the integrated interdiffusion coefficients can be compared to the activation energy for growth of the intermetallic phases to identify the influence of the end member compositions on the growth rates of the intermetallic phases.

Average effective interdiffusion coefficients for each phase were also determined using the relation (Dayananada, 1993)

$$\tilde{D}_i^{eff} = \frac{\int_{x_1}^{x_2} \tilde{J}_i dx}{\Delta C} \quad (i=1,2,3,...,n) \qquad 26)$$

where x_1 and x_2 refer to the end positions of a relevant phase.

The intrinsic diffusion coefficients for component *i* were calculated based on accumulated intrinsic fluxes determined from the location of the marker plane, x_m, via Heumann's method (Heumann, 1952). The accumulated intrinsic flux, A_i, is defined by

$$A_i = \int_0^t J_i dt = -\int_0^t D_i \frac{\partial C_i}{\partial x} dt \quad (i=Mg \text{ or } Al) \qquad (27)$$

Determination of the accumulated intrinsic diffusion flux for component *i* allows for the calculation of the intrinsic diffusion coefficients at the marker plane using the relation

$$D_i = -\frac{A_i}{2t\left[\frac{\partial C_i}{\partial x}\right]_{x_m}} \quad (i = Mg \text{ or } Al) \tag{28}$$

Following the determination of the interdiffusion and intrinsic diffusion coefficients, the pre-exponential factor, D_o and the activation energy, Q_i, were found using the Arrhenius expression (Eq. (19)).

3.2.3 Impurity and self-diffusion

Self-diffusion and impurity diffusion experiments from thin film samples can be analyzed in one direction, with respect to time. The thin film geometry provides an instantaneous planar source initial condition requiring that at time t=0, the diffusion species is deposited on the plane, x=0, and allowed to diffuse for a time t>0 and is given by

$$C(x, 0) = M\delta(x) \tag{29}$$

where M is the number of particles diffusing per unit area and $\delta(x)$ is the Dirac delta function. A solution to the diffusion equation, or Fick's second law (Eq. (4)) for constant diffusivity for the given specimen geometry is given by the Gaussian solution

$$C(x,t) = \frac{M}{\sqrt{\pi Dt}} \exp\left(-\frac{x^2}{4Dt}\right) \quad (30)$$

where *C* is the concentration, *D* is the diffusion coefficient and *t* is the time. To extract the diffusion coefficient, manipulation of the SIMS depth profile obtained is performed. A plot of the natural log of concentration (fraction of isotope) versus the square of the distance is made. This plot results in a straight line with the slope equal to -1/4Dt, as seen in Figure 14, from which, with a known *t*, the diffusion coefficient, *D*, can be calculated. This approach is known as the tracer method.

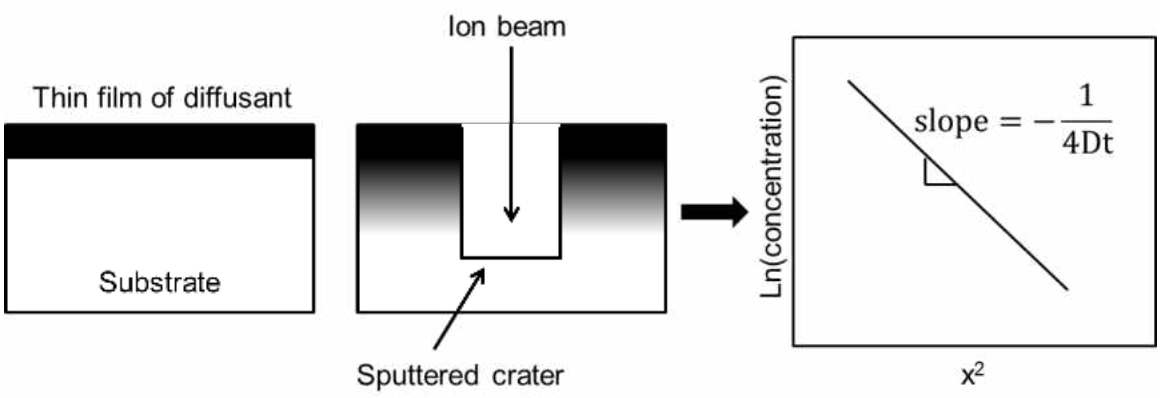

Figure 14: Schematic illustration of the tracer method using SIMS depth profiling. Initially, a thin layer of diffusant is deposited on the substrate; the specimen is then annealed and depth profiled with SIMS. The data is then plotted in the coordinates shown in the graph and the diffusion coefficient, D, is found from the slope and annealing time.

4 RESULTS

4.1 Interdiffusion analysis: Magnesium-Aluminum system

4.1.1 Diffusion microstructures and intermetallic phase layer growth

Backscatter electron micrographs from the three diffusion couples and the corresponding concentration profiles determined by EPMA are presented in Figure 15. Two discernable intermetallic layers were observed, identified as the intermetallic phases, γ-$Mg_{17}Al_{12}$ (near the Mg) and β-Mg_2Al_3 (near the Al) based on analysis by XEDS and the phase diagram (Okamoto, 1998) in Figure 12. In all diffusion couples the ε-$Mg_{23}Al_{30}$ phase, present on the phase diagram between the β- and γ-phase fields, was not observed. A large solubility range for the γ-$Mg_{17}Al_{12}$ phase was observed in all couples in accordance with the phase diagram. The β-phase was thicker than the γ-phase at all temperatures examined. This result agrees well with those reported by Brubaker and Liu (Brubaker & Liu, 2004), Funamizu and Watanabe (Funamizu & Watanabe, 1972) and Tanguep Njiokep *et al.* (Tanguep Njiokep, Salomon, & Mehrer, 2001).

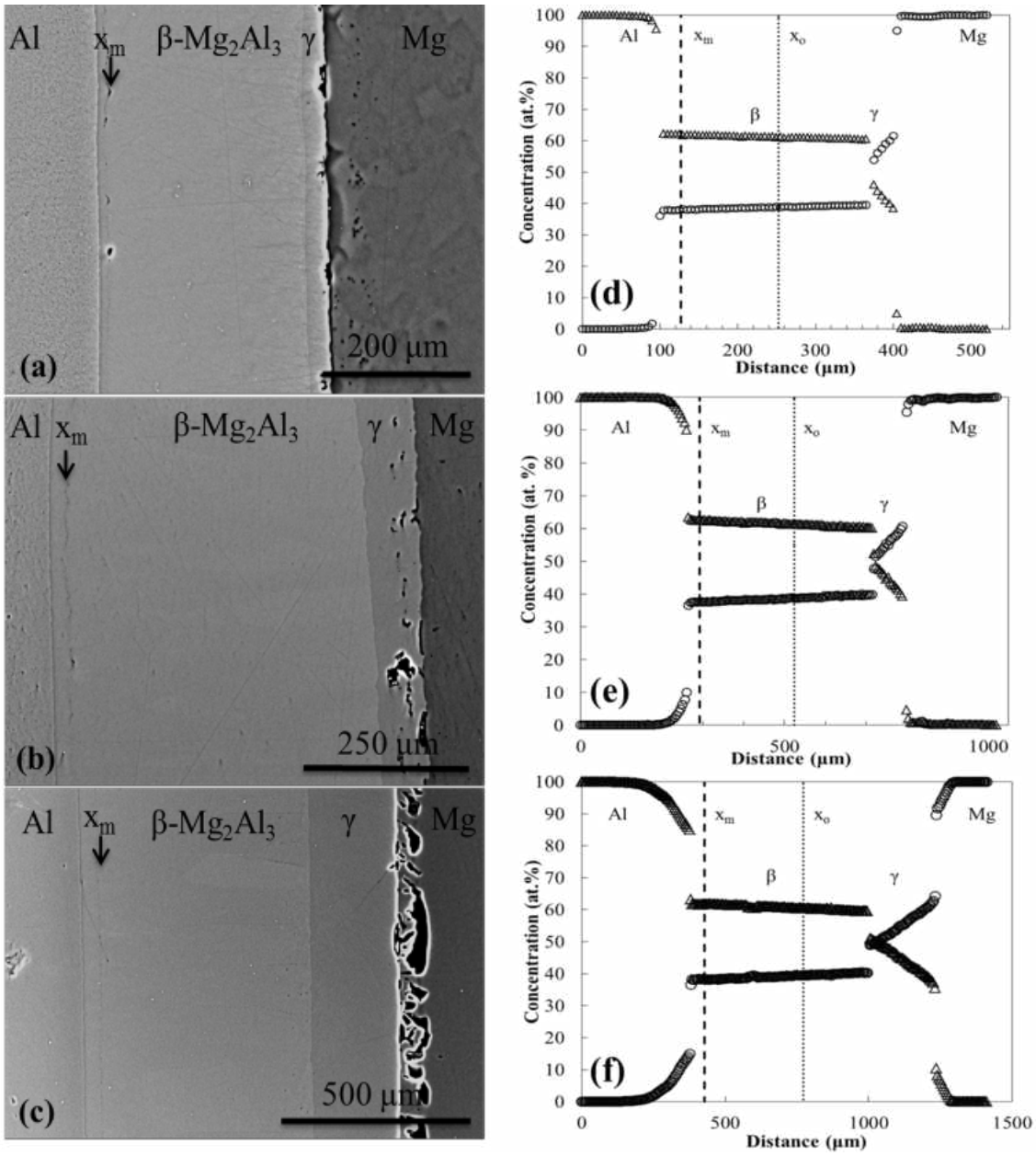

Figure 15: Backscatter electron micrographs of Mg vs. Al diffusion couples at (a) 573K for 30 days, (b) 623K for 15 days, and (c) 673K for 10 days, and electron microprobe concentration profiles at (d) 573K for 30 days, (e) 623K for 15 days, and (f) 673K for 10days.

A minimum of 15 random-location measurements were made to determine the thickness of each intermetallic layer from backscatter electron micrographs using image analysis. Parabolic growth constants for both the β-Mg_2Al_3 and γ-$Mg_{17}Al_{12}$ intermetallic phases were determined using Eq. (20) due to previous investigators (Funamizu & Watanabe, 1972) (Tanguep Njiokep, Salomon, & Mehrer, 2001) reporting the growth of both intermetallic phases as parabolic in the temperature range studied. The intermetallic phase layer thicknesses and parabolic growth constants are reported in Table 6. The β-phase, with limited solubility, grew faster than the γ-phase with larger solubility. The Arrhenius temperature dependence of the growth rate constant, k_p, for both intermetallic phases is presented in Figure 16. Table 6 also reports the activation energy and pre-exponential factor for the growth of the γ-$Mg_{17}Al_{12}$ and β-Mg_2Al_3 phases calculated using Eq. (21). Activation energies reported by Funamizu and Watanabe (Funamizu & Watanabe, 1972) and Tanguep Njiokep et al. (Tanguep Njiokep, Salomon, & Mehrer, 2001) are given for comparison. The activation energy calculated for growth of the β-phase is slightly higher than those reported by Funamizu and Watanabe and Tanguep Njiokep *et al*. The activation energy for the growth of γ-phase is slightly higher than the value reported by Funamizu and Watanabe but, agrees well to the value reported by Tanguep Njiokep *et al*.

Table 6: Thickness measurements from SEM and EPMA comparison, parabolic growth constants, pre-exponential factors and activation energies for growth.

		γ-$Mg_{17}Al_{12}$	β-Mg_2Al_3
x (μm)	673K/10 days	226 (2)	595 (3)
	623K/15 days	77 (6)	481 (5)
	573K/30 days	29 (2)	273 (2)
k_p (m^2/s)	673K/10 days	$2.9x10^{-14}$	$2.1x10^{-13}$
	623K/15 days	$2.3x10^{-15}$	$8.9x10^{-14}$
	573K/30 days	$1.7x10^{-16}$	$1.4x10^{-14}$
k_o (m^2/s)		0.18	$1.1x10^{-6}$
Q_k (kJ/mol)		165.0 (This study)	85.5 (This study)
		143.1 (Funamizu & Watanabe, 1972)	62.3 (Funamizu & Watanabe, 1972)
		165.0 (Tanguep Njiokep, Salomon, & Mehrer, 2001)	69.0 (Tanguep Njiokep, Salomon, & Mehrer, 2001)

Note: Values in parenthesis are standard deviation

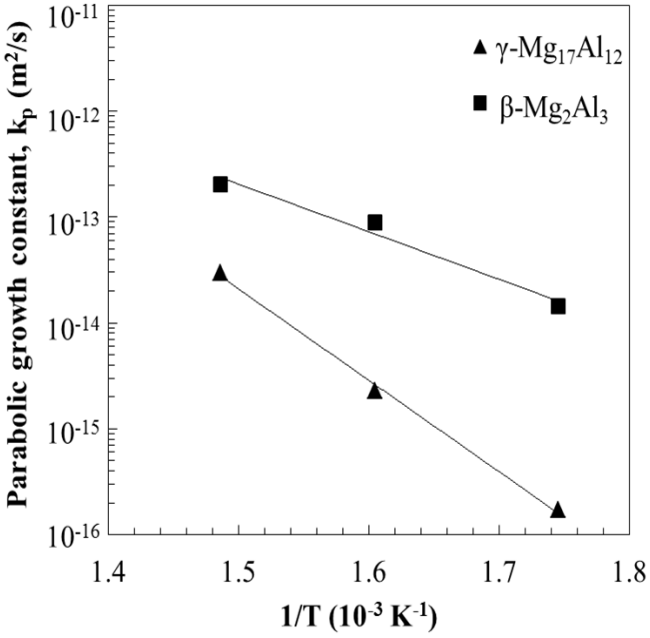

Figure 16: Temperature-dependence of the parabolic growth constants for the γ-$Mg_{17}Al_{12}$ and β-Mg_2Al_3 phases determined from layer thickness measurements after diffusion annealing.

The Kirkendall marker plane, x_m, is clearly demarcated in Figure 15, in the β-phase near the β/Al (ss) interface. The location of the marker plane was confirmed by extensive XEDS analysis, where the presence of oxygen was confirmed qualitatively. The location of the marker plane is the same as those reported by Funamizu and Watanabe (Funamizu & Watanabe, 1972) and by Tanguep Njiokep *et al* (Tanguep Njiokep, Salomon, & Mehrer, 2001).

4.1.2 Interdiffusion and intrinsic diffusion analysis

Concentration-dependent interdiffusion coefficients were calculated using the Boltzmann-Matano method, described by Eqs. (22) through (24), for the Mg-solid solution, Al-solid solution, γ-$Mg_{17}Al_{12}$, and β-Mg_2Al_3 phases from all three diffusion couples. Figure 17 presents the concentration-dependent interdiffusion coefficients as a function of Mg concentration determined in this study. Interdiffusion coefficients of the β-phase are an order of magnitude higher than those of the γ-phase, which are an order of magnitude higher than those of the Mg (ss) and Al (ss). As seen from Figure 17, the variation in interdiffusion coefficients as a function of concentration is negligible for the β-Mg_2Al_3 phase, while there is a slight decrease in interdiffusion coefficient with an increase in Mg concentration in the γ-$Mg_{17}Al_{12}$ phase. In both the Al (ss) and Mg (ss), interdiffusion coefficients increased with an increase in their respective alloying additions.

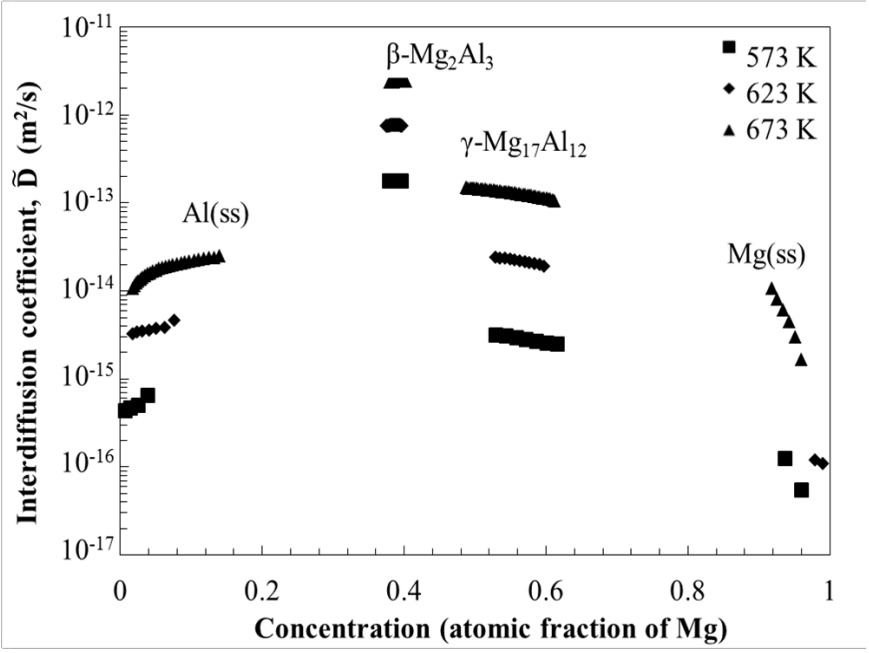

Figure 17: Interdiffusion coefficients as a function of Mg concentration for the Al solid solution, β-Mg_2Al_3 phase, γ-$Mg_{17}Al_{12}$ phase and Mg solid solution.

The integrated interdiffusion coefficient, $\widetilde{D}_{i,\Delta x}^{int}$, was calculated using Eq. (25) for the Al solid solution, the β- and γ-phases and the Mg solid solution for each diffusion couple as presented in Table 7. The pre-exponential factor and activation energy for the integrated interdiffusion coefficients were calculated and are shown in Figure 18. The Mg solid solution had the highest activation energy, followed by the γ-$Mg_{17}Al_{12}$ phase, the Al solid solution, and lastly, the β-Mg_2Al_3 phase. These integrated interdiffusion coefficients are material properties and will be the same, irrespective of the starting end member compositions of the diffusion couple.

Table 7: Integrated interdiffusion coefficients for the Mg solid solution, γ-$Mg_{17}Al_{12}$ phase, β-Mg_2Al_3 phase, and the Al solid solution.

	Integrated Interdiffusion Coefficients, $\widetilde{D}_{i,\Delta x}^{int}$ (m^2/s)			
Temperature	Mg (ss)	γ-$Mg_{17}Al_{12}$	β-Mg_2Al_3	Al (ss)
673K	$4.3x10^{-16}$	$2.0x10^{-14}$	$5.6x10^{-14}$	$2.5x10^{-16}$
623K	$8.0x10^{-18}$	$1.7x10^{-15}$	$1.8x10^{-14}$	$2.4x10^{-17}$
573K	$5.3x10^{-19}$	$2.0x10^{-16}$	$2.9x10^{-15}$	$2.6x10^{-18}$

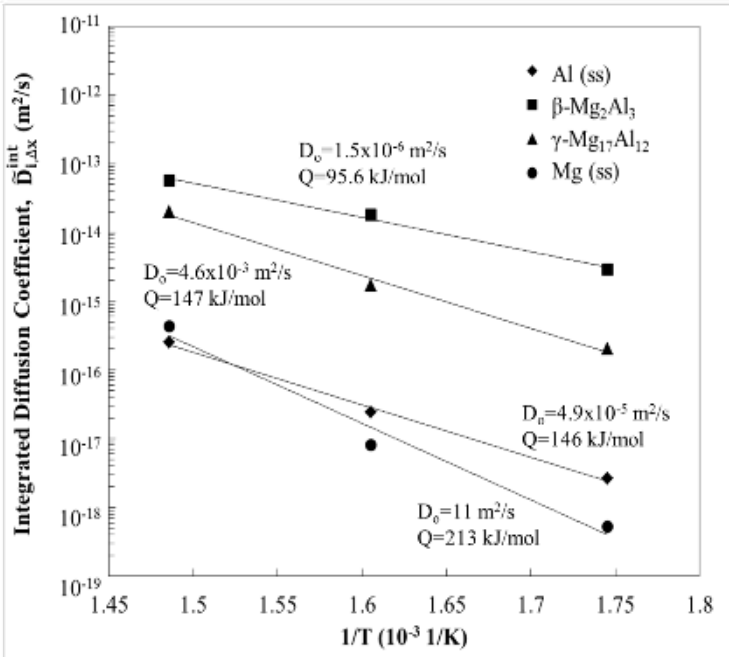

Figure 18: Temperature-dependence of integrated interdiffusion coefficients for the Al solid solution, β-Mg_2Al_3 phase, γ-$Mg_{17}Al_{12}$ phase, and the Mg solid solution.

Average effective interdiffusion coefficients were determined using Eq. (26) to calculate the activation energy and pre-exponential factor for interdiffusion in each phase. The activation energies for interdiffusion were calculated from average effective interdiffusion coefficients because the concentration difference obtained from the EPMA

profiles were reliable enough to use. Average effective interdiffusion coefficients are reported in Table 8. Figure 19 presents the average effective interdiffusion coefficients for each phase as a function of temperature. The pre-exponential factors and activation energies for interdiffusion coefficients are reported in Table 9. The activation energy for the interdiffusion coefficient in the β-Mg_2Al_3 phase is smaller than that of γ-$Mg_{17}Al_{12}$, Al (ss) and Mg (ss) phases. Also noted is the greater activation energy for interdiffusion of Al in Mg (ss) than Mg in Al (ss).

Table 8: Average effective interdiffusion coefficients for the Mg solid solution, γ-$Mg_{17}Al_{12}$, β-Mg_2Al_3 and Al solid solution phases.

	Average Effective Interdiffusion Coefficients, $\widetilde{D}_i^{eff}$ (m^2/s)			
Temperature	Mg (ss)	γ-$Mg_{17}Al_{12}$	β-Mg_2Al_3	Al (ss)
673K	$4.9x10^{-15}$	$1.3x10^{-13}$	$2.4x10^{-12}$	$1.9x10^{-14}$
623K	$2.3x10^{-16}$	$2.2x10^{-14}$	$7.5x10^{-13}$	$3.3x10^{-15}$
573K	$1.4x10^{-17}$	$2.8x10^{-15}$	$1.8x10^{-13}$	$7.1x10^{-16}$

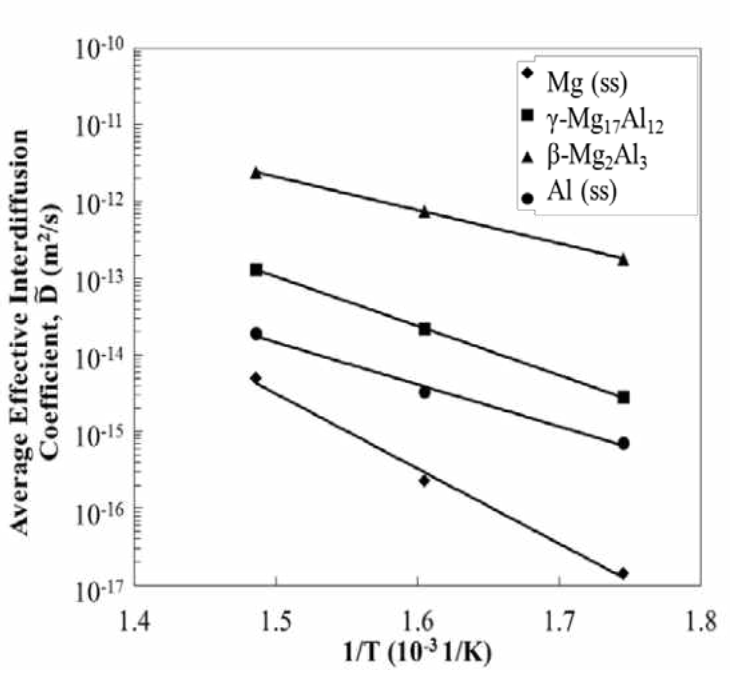

Figure 19: Temperature dependence of the average effective interdiffusion coefficients for the Mg solid solution, γ-$Mg_{17}Al_{12}$ phase, β-Mg_2Al_3 phase, and the Al solid solution.

Table 9: Activation energies and pre-exponential factors for average effective interdiffusion coefficients for the Mg solid solution, γ-$Mg_{17}Al_{12}$ phase, β-Mg_2Al_3 phase, and the Al solid solution.

	Mg (ss)	γ-$Mg_{17}Al_{12}$	β-Mg_2Al_3	Al (ss)
Q (kJ/mol)	187.1	123.1	83.1	104.8
D_o (m^2/s)	1.45	$4.6x10^{-4}$	$6.8x10^{-6}$	$2.5x10^{-6}$

The location of the Kirkendall marker plane, x_m, was clearly identified in the β-Mg_2Al_3 phase in all three diffusion couples, as presented in Figure 15. The concentration gradient at the marker plane, reported in Table 10, was reliable enough to calculate the intrinsic diffusion coefficients of Mg and Al in the β-Mg_2Al_3 phase based on Heumann's

analysis (Heumann, 1952) described by Eqs. (27) and (28). The intrinsic diffusion of Al in the β-phase is clearly much faster than Mg as seen in Table 10. The temperature-dependence of the intrinsic diffusion coefficients for Mg and Al in the β-Mg_2Al_3 phase at the marker composition of Mg-62 at.% Al is presented in Figure 20. The pre-exponential factor and activation energy for the intrinsic diffusion coefficient of Mg and Al in the β-Mg_2Al_3 phase at the specified composition is also given in Figure 20.

Table 10: Intrinsic Diffusion Coefficients for Mg and Al at the approximate marker plane composition of Mg-62 at.% Al in the β-Mg_2Al_3 phase.

Temperature	Concentration (at.% Mg)	Concentration Gradient $\left[\partial C_{Mg}/\partial x\right]_{x_m}$ (mol/m^4)	Intrinsic Diffusion Coefficients, D_i (m^2/s)	
			D_{Mg}	D_{Al}
673K	38.2	7.9×10^{7}	1.9×10^{-14}	2.9×10^{-13}
623K	37.5	1.1×10^{8}	3.9×10^{-15}	8.8×10^{-14}
573K	38.0	2.6×10^{8}	8.4×10^{-16}	8.9×10^{-15}

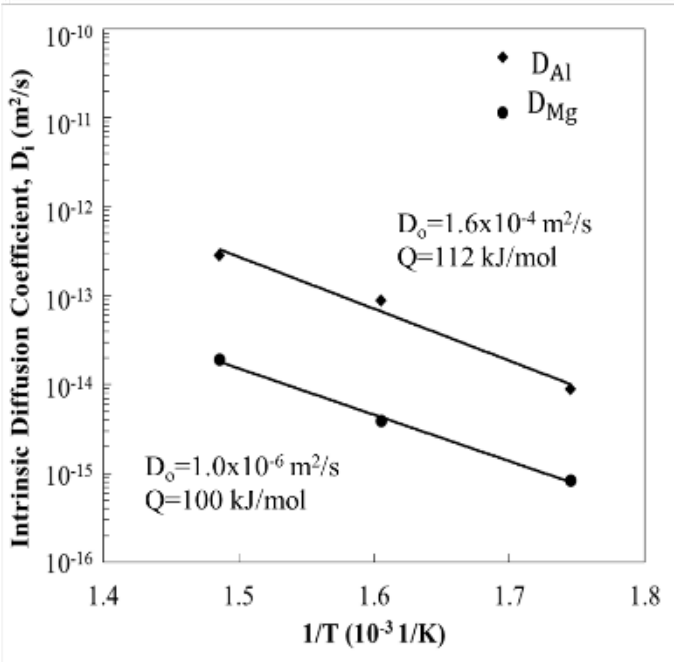

Figure 20: Temperature-dependence of the intrinsic diffusion coefficients of Al and Mg at the marker plane composition of Mg-62 at.% Al in the β-Mg_2Al_3 phase.

4.2 Self- and impurity diffusion analysis

4.2.1 Aluminum impurity diffusion in polycrystalline magnesium

An Al film approximately 500nm thick was deposited on seven (7) Mg substrates under the conditions provided in Chapter 3.1.3. One as-deposited specimen was utilized to verify the film thickness. The as-deposited sample was depth profiled with the SIMS, presented in Figure 21, and confirms the thickness of the Al film to be around 500 nm. Two samples each were annealed at 573, 623, and 673K (300, 350 and 400°C) for 120,

30 and 30 minutes, respectively. Up to three spots on each sample were depth profiled with SIMS to certify reproducibility in the same sample as well as between samples.

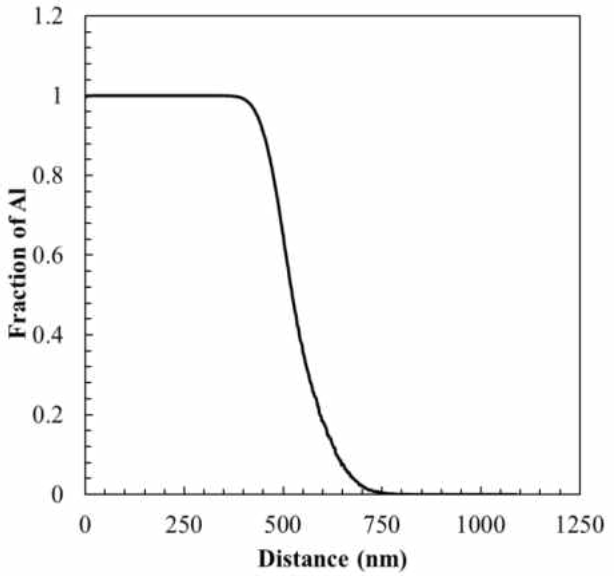

Figure 21: SIMS depth profile of the as-deposited Al thin film on a Mg substrate.

A typical depth profile at each temperature is presented in Figure 22. As evident in Figure 22, the penetration depth increases dramatically from 573 to 673K. The dilute end (~<10^2 SIMS intensity of Al) of each profile was plotted in the natural logarithm of SIMS intensity versus the square of the penetration depth. The actual concentration at this dilute level can be assumed to vary linearly with SIMS intensity and therefore, the SIMS intensity can be used directly to calculate the Al impurity diffusion coefficient (Petuskey, 1983). Figure 22 also presents the natural logarithm of the fraction of Al versus the square of the penetration depth for the depth profiles. The good linear fit

exhibited by these profiles is verification that the application of the Gaussian thin film solution is appropriate.

Table 11 reports the Al impurity diffusion coefficients for each spot on each sample as well as the average diffusion coefficient for each temperature. From these average values, the pre-exponential factor and activation energy were calculated as presented in Figure 23.

Table 11: Al impurity diffusion coefficients in Mg.

Sample	Al impurity diffusion coefficient in Mg, D_{Al}^{Mg} (m^2/s)	Average D_{Al}^{Mg} (m^2/s)
	573K/120 minutes	
3_1	2.53×10^{-17}	2.7×10^{-17} (3.4×10^{-18})
3_2	2.94×10^{-17}	
3_3	2.14×10^{-17}	
4_1	2.81×10^{-17}	
4_2	2.96×10^{-17}	
	623K/30 minutes	
1_3	6.10×10^{-16}	5.3×10^{-16} (1.0×10^{-16})
2_2	4.60×10^{-16}	
	673K/30 minutes	
2_1	3.59×10^{-15}	3.3×10^{-15} (9.6×10^{-16})
2_2	4.01×10^{-15}	
3_1	2.18×10^{-15}	

Note: Values in parenthesis are standard deviation.

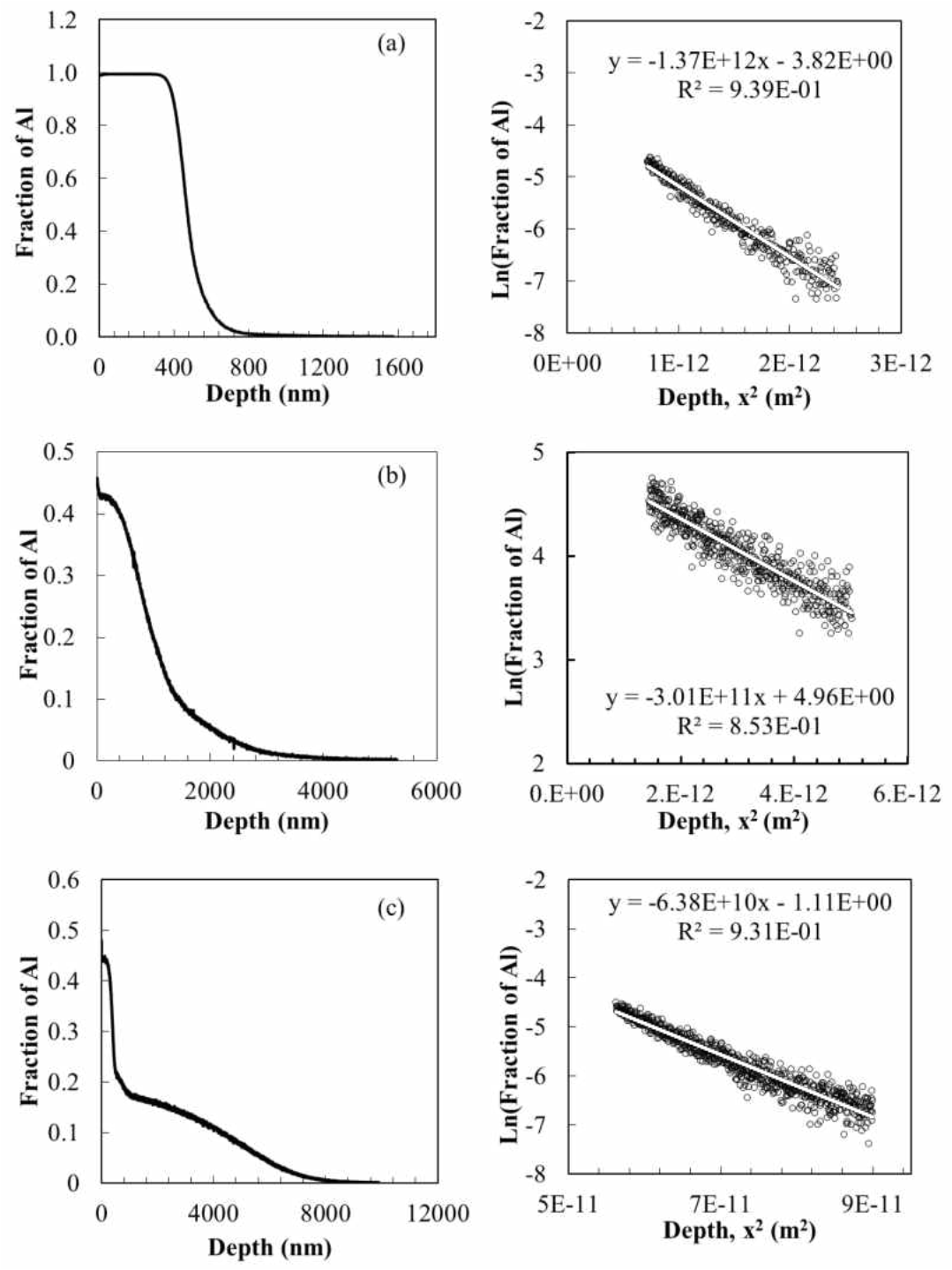

Figure 22: Typical SIMS depth profiles and Gaussian profile fits for (a) 573K for 120 minutes, (b) 623K for 30 minutes, and (c) 673K for 30 minutes.

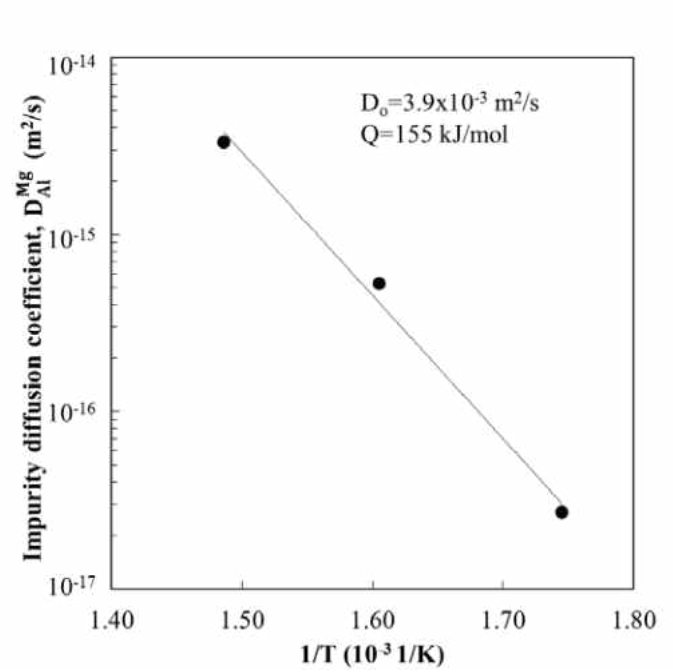

Figure 23: Temperature-dependence of Al impurity diffusion in polycrystalline Mg measured from SIMS depth profiles.

4.2.2 Self-diffusion of the stable isotope ^{25}Mg in polycrystalline magnesium

A thin film, approximately 100nm, of ^{25}Mg was deposited on five (5) polycrystalline Mg substrates under the conditions described in Chapter 3.1.2. One as-deposited specimen was depth profiled with SIMS to verify the ^{25}Mg film thickness as shown in Figure 24. One SIMS spot on each sample was profiled as well as a total of five spots on the 623K sample to verify consistency in obtaining the diffusion coefficient. There was a 10% uncertainty attributed with calculating the diffusion coefficient between the 5 spots.

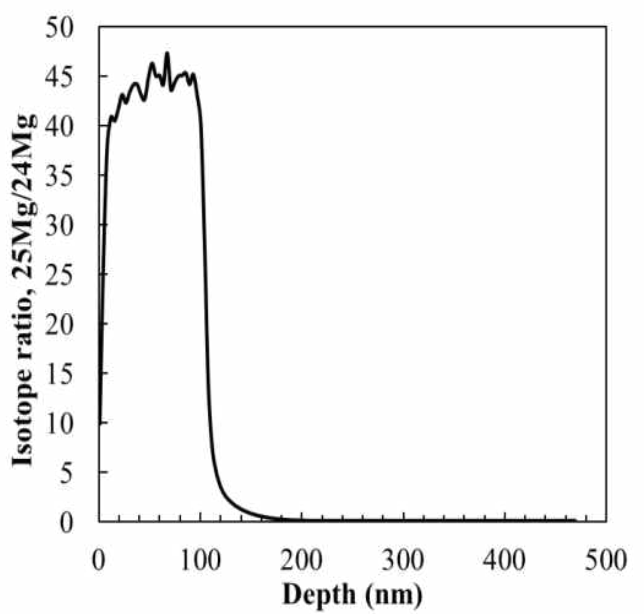

Figure 24: As-deposited SIMS depth profile for 25Mg film on polycrystalline Mg substrate.

The depth profiles for each specimen are shown in Figure 25 with their corresponding Ln(^{25}Mg/^{24}Mg) vs. x^2 plots. The calculated self-diffusion coefficients are reported in Table 12. The temperature-dependence of the calculated self-diffusion coefficients are presented in Figure 26 along with reported literature values of Mg self-diffusion. The pre-exponential factor and activation energy for self-diffusion are also given in Figure 26. It is evident that the presently calculated values are higher in magnitude than the literature values. The possible reasons for this discrepancy will be discussed in Chapter 5.2.2.

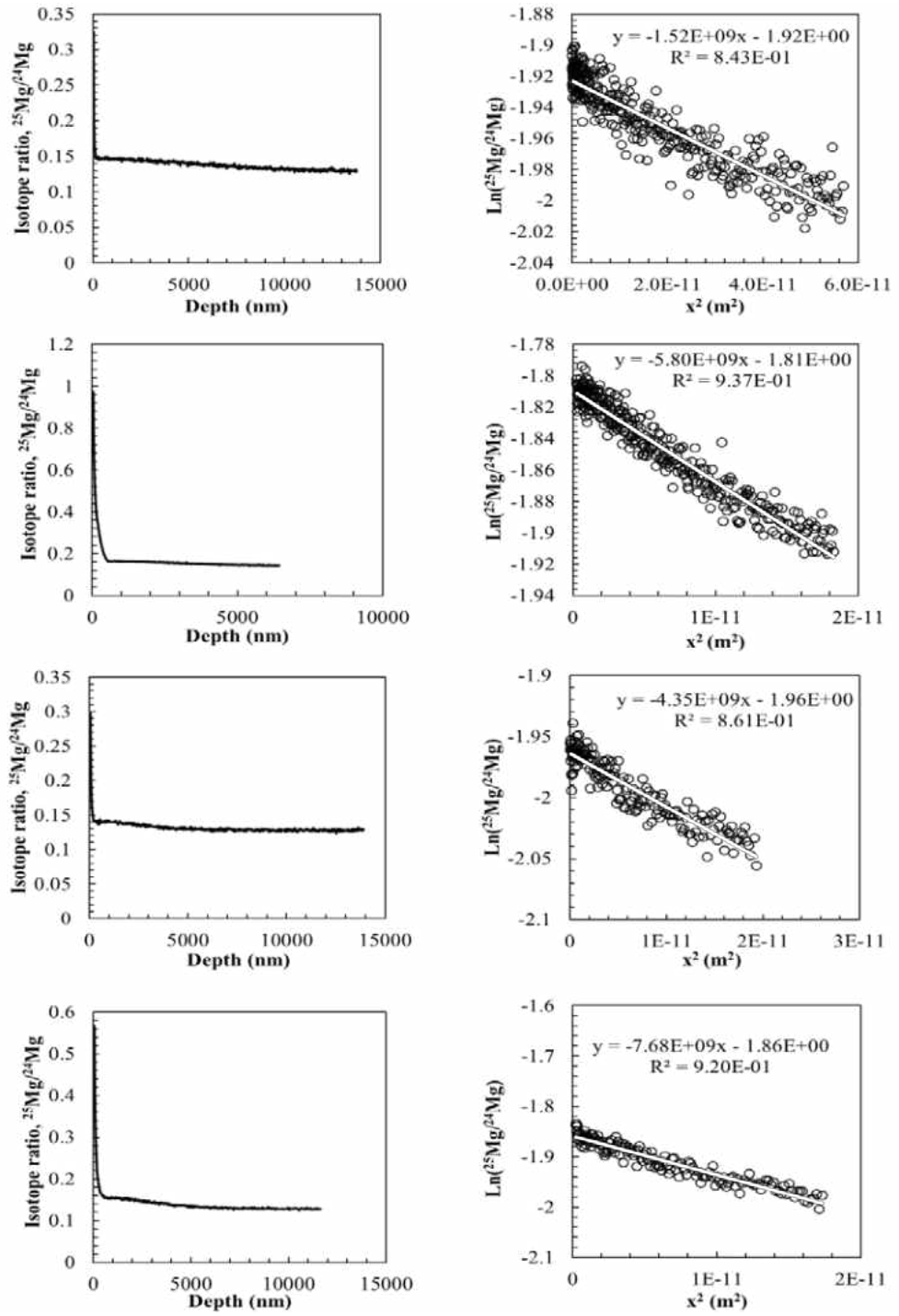

Figure 25: SIMS depth profiles and Gaussian fit profiles for Mg self-diffusion at a) 673K 30 minutes, (b) 623K 60 minutes, (c) 573K for 240 minutes, and (d) 523K for 720 minutes.

Table 12: Calculated Mg self-diffusion coefficients in polycrystalline Mg from SIMS depth profiles.

Specimen	D_{self} (m^2/s)
673K/30 min.	9.13×10^{-14}
623K/60 min.	1.19×10^{-14}
573K/240 min.	4.00×10^{-15}
523K/720 min.	7.53×10^{-16}

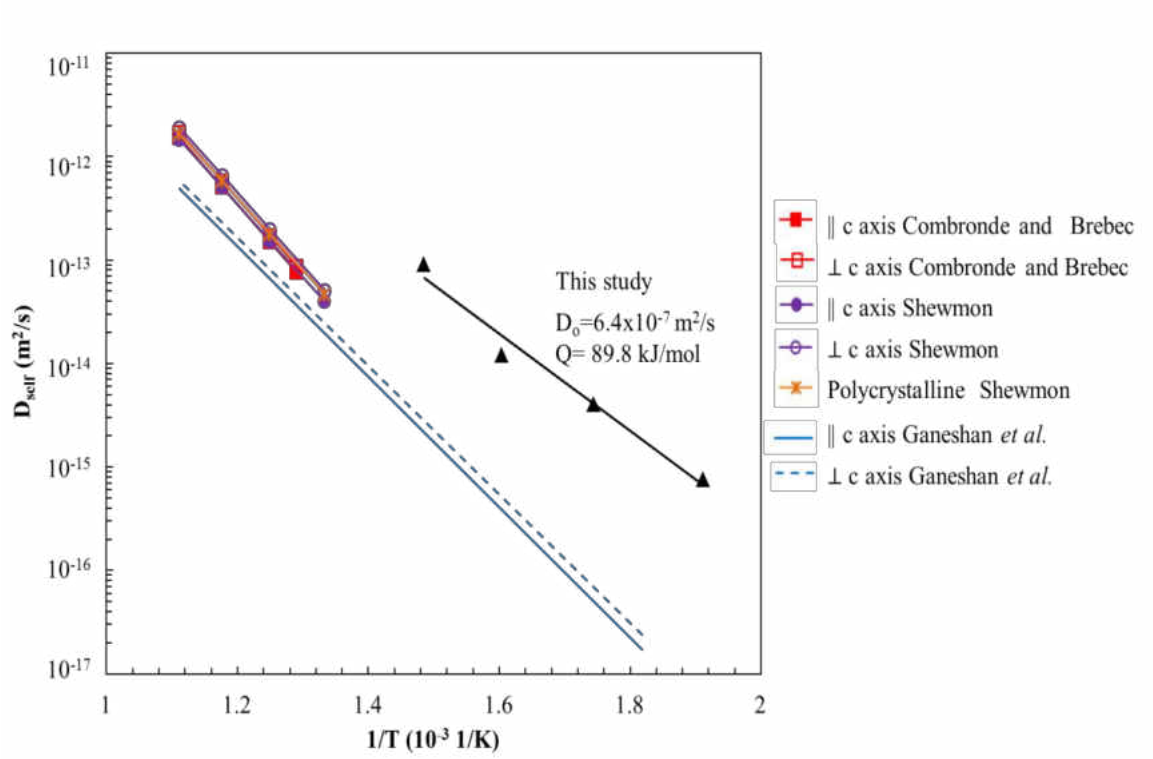

Figure 26: Temperature-dependence of Mg self-diffusion from this study and reported literature values.

5 DISCUSSION

5.1 Interdiffusion analysis: Magnesium-Aluminum system

5.1.1 Diffusion microstructural features

There are still existing discrepancies regarding the equilibrium phase diagram for the binary Mg-Al system in the composition range of 40-60 at.% Al and the temperature range above 250°C, especially regarding the ε-phase field, which is located in between the β-and γ-phase fields. In the diffusion microstructures examined in this study, the ε-phase was not observed. A diffusion study of the Mg-Al system by Brubaker and Liu (Brubaker & Liu, 2004) in the temperature range of 633 to 693K reported the existence of a thin layer of the ε-phase in diffusion couples annealed at 640K and 633K. In contrast, an earlier investigation of the system in the temperature range of 598K to 698K by Funamizu and Watanabe (Funamizu & Watanabe, 1972) reported that the ε-phase did not develop in any of their diffusion couples. In the study by Tanguep Njiokep *et al*. (Tanguep Njiokep, Salomon, & Mehrer, 2001), it was stated that some diffusion couples developed a very thin layer of the ε-phase observed by optical microscopy but was not verified. The absence of the ε-phase may be explained from a framework that considers solubility range, diffusion coefficients, and thermodynamics (Gibbs, 1966) (Kajihara, 2004) (Kidson, 1961) (Pretorius, Marais, & Theron, 1993).The ε-phase has a narrow range of solubility (1.3 at. %) (Brubaker & Liu, 2004) (Okamoto, 1998), and may be thermodynamically and kinetically unfavorable to nucleate and/or grow relative to the β- and γ-phases. The melting temperature of the ε-phase is lower than its surrounding

phases (β and γ). It is evident as well, from Table 8 and Figure 19, that the β-and γ-phases have high diffusivities, possibly much higher than that of the ε-phase, therefore making intermixing of the system by the nucleation and growth of this phase unfavorable.

Figure 15 shows representative microstructures of each of the diffusion couples in this study. The porosity on the Mg side of the couples may be due to the intrinsic diffusion behavior of Mg and Al. The Mg in the Mg (ss) may migrate faster into the adjoining γ-phase than Al is released from the γ-phase into the Mg (ss). The porosity was most evident in the couple annealed at 673K (400°C), and the interdiffusion coefficients in the Mg (ss) phase varies greatly with temperature as shown in Figure 17. However, the marker plane was not located in the Mg (ss) in this study, warranting further investigation of intrinsic diffusion within the Mg (ss).

5.1.2 Intermetallic phase layer growth

The activation energy for growth determined from the thickness measurements for the β-phase is markedly lower than that for the γ-phase as reported in Table 6. This difference in growth activation energies is consistent with the trend reported by Funamizu and Watanabe (Funamizu & Watanabe, 1972), Tanguep Njiokep (Tanguep Njiokep, Salomon, & Mehrer, 2001). Analysis of the concentration profiles has also demonstrated that the β-phase has the higher interdiffusion coefficients and the lower

activation energy for interdiffusion, although its solubility range is smaller than the γ-phase. In other words, the γ-phase has the larger solubility, but with lower interdiffusion coefficients and higher activation energy, it has developed a much thinner layer as shown by the micrographs in Figure 15.

Activation energies determined from the growth constants using Eqs. (20) and (21) can be compared to those determined from the integrated interdiffusion coefficients from Eqs. (23) and (25) and the average effective interdiffusion coefficients using Eqs. (23) and (26). These values are reported in Table 6 and Table 9 and Figure 18. For the fast growing β-phase, these three values have an average value of 88.1$\pm$ 6.7kJ/mole, indicating the growth of the phase is predominately diffusion controlled. However, for the slower-growing γ-phase, activation energy for growth based on thickness measurements is ~165 kJ/mole, while that for integrated interdiffusion is 147kJ/mole and only ~123 kJ/mole for the average effective interdiffusion. This difference indicates that the growth of γ-phase may not be purely diffusion-controlled and may not follow the assumed parabolic rate, even though previous studies ((Funamizu & Watanabe, 1972) (Tanguep Njiokep, Salomon, & Mehrer, 2001)) observed the $\sqrt{t}$ dependence. This difference between activation energies may also arise from the temperature-dependence of the homogeneity range of the γ-phase which is much wider at higher temperatures.

It has been suggested that the rate of intermetallic phase growth depends on the terminal compositions (e.g., impurity level) and the number of phases that form in the diffusion couple (Wagner, 1969) (Dybkov, 2002). In this study, high purity Mg (99.9%) and Al (99.999%) were employed and all diffusion couples developed well-defined thermodynamically-constrained planar interfaces between each phase. The integrated interdiffusion coefficients calculated are a property of the material and will be the same regardless of the end member compositions (Dybkov, 2002) (Wagner, 1969).

5.1.3 Interdiffusion and intrinsic diffusion

Interdiffusion coefficients in the β-phase remained relatively constant as a function of concentration and decreased slightly with an increase in Mg concentration in the γ-phase as presented in Figure 17. Interdiffusion coefficients for both terminal solid solutions increased with an increase in alloying concentration. Activation energies were also determined based on average effective interdiffusion coefficients for the two terminal solutions, e.g., Mg interdiffusion in Al (ss) and Al interdiffusion in Mg (ss). Al interdiffusion in Mg (ss) requires markedly higher activation energy than Mg interdiffusion in Al (ss) as reported in Table 9. The solubility limits of both terminal solid solutions as well as the sizes of both Mg and Al atoms may possibly contribute to the observed difference in activation energies. Al has at most, 18.6 at% solubility for Mg while Mg has 11.5 at% solubility for Al.

From binary diffusion theory, it is somewhat common to observe the element with the lower melting temperature to diffuse faster. Mg and Al have very close melting temperatures, 923K and 933K, respectively. It is evident, however, from the diffusion microstructures and marker plane location that Al migrates faster in this binary system. Interdiffusion coefficients in the β-phase, presented in Table 8, are higher than those in the γ-phase. The β- and γ-phases both have cubic crystal structures, however, the β-phase has a very large, complex cubic structure (Pearson symbol cF1168) (Samson, 1965) while the γ-phase has a smaller cubic structure (Pearson symbol cI58) (Okamoto, 1998). The larger size of the β-phase may develop a higher concentration of defects and thus have a correspondingly larger diffusivity. The structural defect in the β-phase has not been clarified, however, from Samson's study of the β-Mg_2Al_3 crystal structure, the number of atoms per unit cell changes from 1165 at 36.23 wt.% to 1178 at 37.83 wt.% Mg. This difference in the number of atoms per unit cell with a deviation in the stoichiometric composition suggests a possible vacancy type defect. According to Samson, the β-Mg_2Al_3 structure exhibits a high amount of inherent disorder in the form of displacement disorder, substitutional disorder and fractional site occupation. Since it is highly possible to have a high defect concentration in the structure, it can be concluded that the diffusivity of Al and Mg atoms within the structure will be somewhat faster. This is supported by the observed large phase thickness and high diffusion coefficients as well as its low activation energy for interdiffusion and growth.

The γ-phase has the ideal stoichiometry of $Mg_{17}Al_{12}$ at 58.6 at.% Mg with the high end of the γ-phase field at 60 at.% Mg and the low end at 45 at.% Mg. The increase in the interdiffusion coefficient in the γ-phase, seen in Figure 17, as the deviation from this stoichiometry increases, suggests the defect concentration also increases. The relatively high interdiffusion coefficients in the γ-phase are somewhat unexpected due to the highly ordered and close packed nature of its crystal structure. Another diffusion mechanism (i.e., anti-sites) could be responsible for the diffusion in this relatively complex structure.

Intrinsic diffusion coefficients of Mg and Al in the β-phase, reported in Table 10, indicate that Al is the faster moving species in the β-Al_3Mg_2 phase. The location of the marker plane, in the β-phase near the β/Al (ss) interface, is also evidence of Al diffusing faster than Mg in this phase due to the Kirkendall effect. This result is in exact agreement with the marker location reported by Funamizu and Watanabe (Funamizu & Watanabe, 1972). Funamizu and Watanabe also concluded that Al intrinsically diffuses faster in the β-phase by observing the rate of the marker plane shift, however, intrinsic diffusion coefficients were reported for only one temperature, 698K, and are approximately one order of magnitude higher than those currently reported for 673K.

Funamizu and Watanabe (Funamizu & Watanabe, 1972) and Tanguep Njiokep *et al*. (Tanguep Njiokep, Salomon, & Mehrer, 2001) determined concentration-independent

(e.g., constant) interdiffusion coefficients via Heumann's analysis (Heumann, 1952). This approach is valid when the intermediate phase formed varies linearly in concentration, and requires the growth constant and solubility limits of the phase under consideration. These "constant" interdiffusion coefficients were determined via Heumann's analysis from the growth constants reported for this study in Table 6 and solubility limits given by the phase diagram shown in Figure 12. They are presented in Figure 27(a) for the β-phase and Figure 27(b) for the γ-phase. The interdiffusion coefficients determined from Heumann's analysis agree well with those determined by Funamizu and Watanabe and Tanguep Njiokep *et al*. for the β-phase. However, there is a significant scatter for the γ-phase, possibly due to the difference in homogeneity range limits of the γ-phase between each studies data or phase diagram used. The average effective interdiffusion coefficients determined from this work, also shown in Figure 27, are higher for both intermetallic phases.

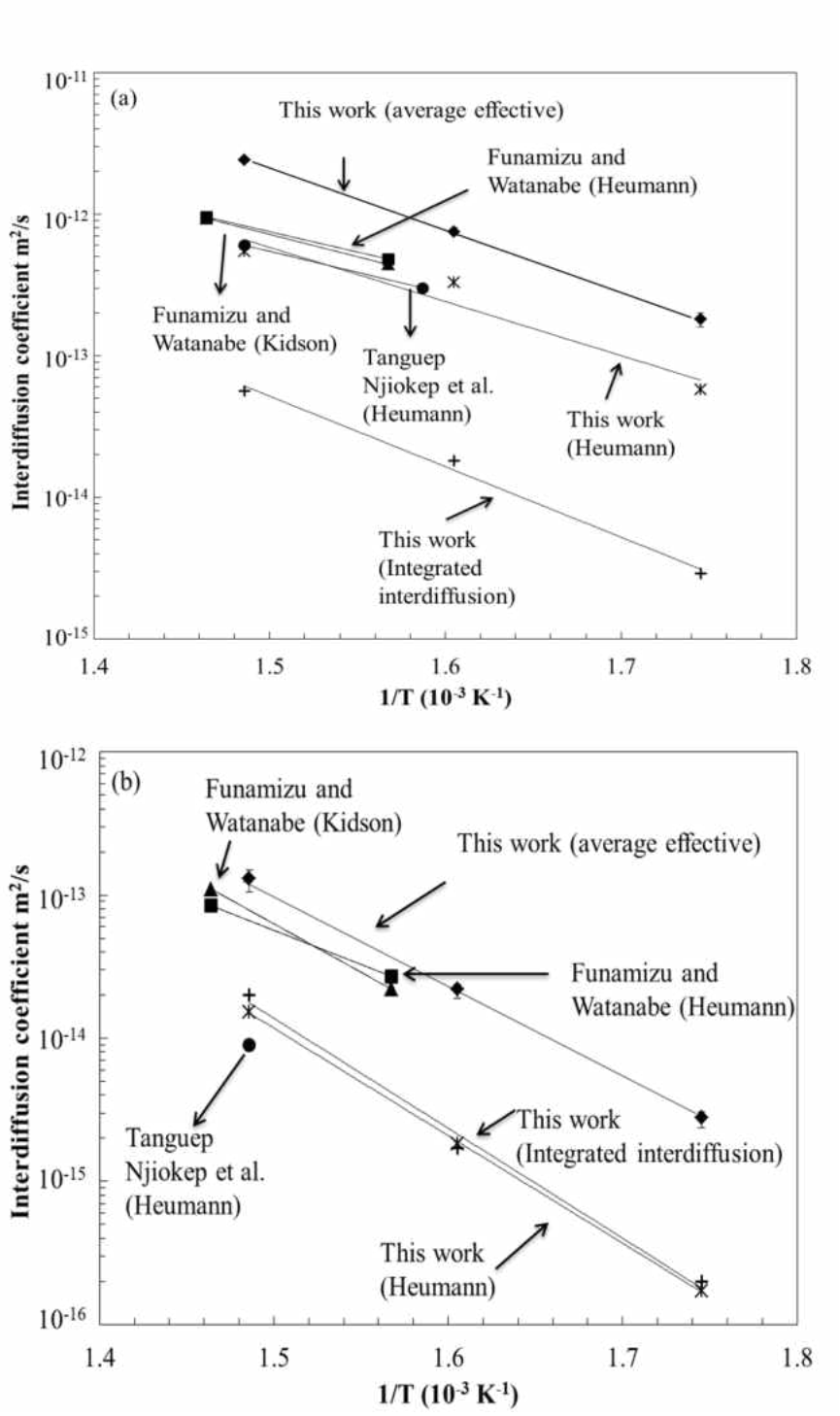

Figure 27: Interdiffusion analysis method comparison for the interdiffusion coefficient in the (a) β-Mg_2Al_3 phase and (b) γ-$Mg_{17}Al_{12}$ phase.

5.1.4 Impurity diffusion estimations

Interdiffusion coefficients in the Al (ss) and Mg (ss) determined as a function of concentration for both terminal solid solutions were extrapolated to near zero at.% of the respective alloying component. These extrapolations may be considered as an estimation of the impurity diffusion coefficients of each solid solution. Care was taken for the extrapolation to exclude experimental measurement of concentrations near the interfaces and terminal ends where the concentration gradients become too uncertain. At 623K and 573K, disregarding the uncertain data left very little to extrapolate for Al impurity diffusion in Mg, D_{Al}^{Mg}. Assuming the variation of the interdiffusion coefficient will be similarly linear near the dilute ends at each temperature, an expression $\mathrm{D}_{\mathrm{Al}}^{\mathrm{Mg}} = \mathrm{D}_{\mathrm{Al}}^{\mathrm{Mg}}(\mathrm{C}_{\mathrm{Al}})$ was determined at 673K and utilized for the extrapolation of D_{Al}^{Mg} at 573K and 623K. A sufficient amount of reliable data points were available to extrapolate the impurity diffusion coefficient of Mg in Al, D_{Mg}^{Al}, for all three temperatures.

Table 13 reports the extrapolated interdiffusion coefficients (i.e., estimated impurity diffusion coefficients), D_{Al}^{Mg} and D_{Mg}^{Al}. The temperature dependence of these impurity diffusion coefficients is presented in Figure 28, along with the self-diffusion coefficients for Al (Lundy & Murdoch, 1962) and Mg (Shewmon & Rhines, Rate of Self-Diffusion in Polycrystalline Magnesium, 1954) (Shewmon, 1956) (Combronde & Brebec, Anisotropie d'autodiffusion du magnesium, 1971). The estimated D_{Mg}^{Al}, is an order of magnitude higher than D_{Al}^{Mg}, and the activation energies for the estimated impurity diffusion

coefficients differ by ~15 kJ/mol. Figure 28 also presents results from Fujikawa and Hirano (Fujikawa & Hirano, 1977) who experimentally determined the tracer diffusion of ^{28}Mg in nearly single crystal Al by using residual activity method after photo-nuclear reaction to prepare carrier-free radioactive ^{28}Mg. The estimated impurity diffusion coefficients for Mg in Al, D_{Mg}^{Al}, from this study agree well to Fujikawa and Hirano, especially at 673K.

Table 13: Extrapolated impurity diffusion coefficients of Al in Mg, D_{Al}^{Mg}, and Mg in Al, D_{Mg}^{Al}, and the corresponding activation energy and pre-exponential factor.

Temperature	D_{Al}^{Mg} (m^2/s)	D_{Mg}^{Al} (m^2/s)
673K	5.5×10^{-16}	9.4×10^{-15}
623K	8.0×10^{-17}	2.9×10^{-15}
573K	1.5×10^{-17}	4.3×10^{-16}
D_o (m^2/s)	4.2×10^{-7}	5.2×10^{-7}
Q (kJ/mol)	114.7	98.9

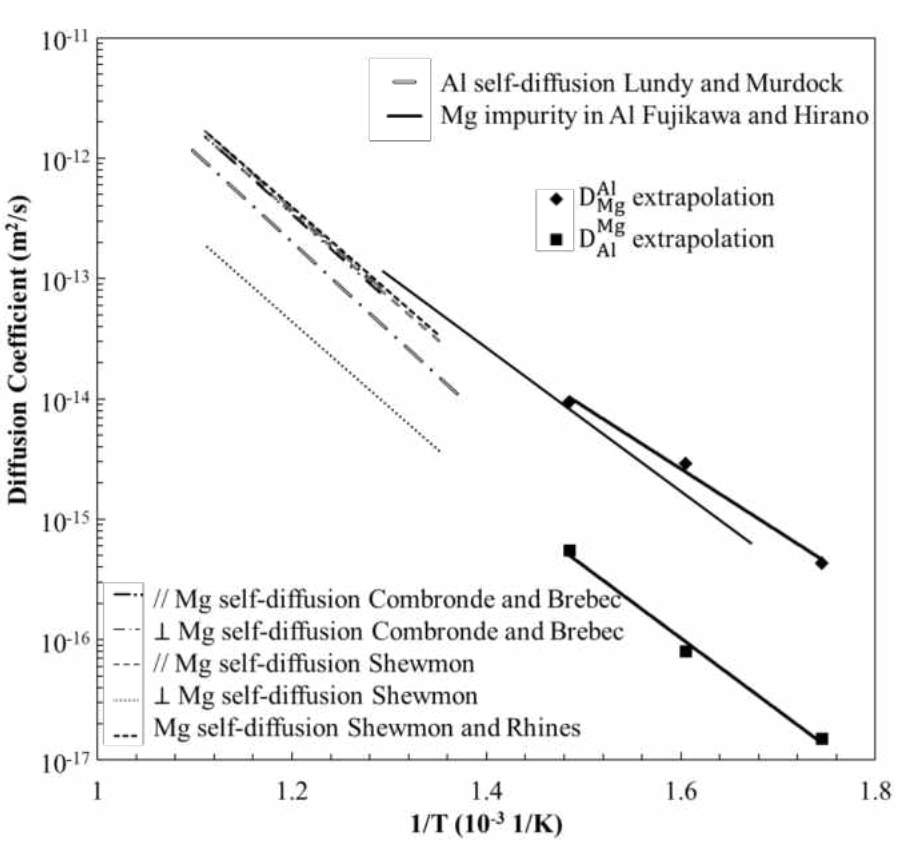

Figure 28: Impurity diffusion extrapolations from interdiffusion data in the Mg and Al solid solutions and comparisons to literature values of Al and Mg self-diffusion and Mg impurity diffusion in Al.

5.1.5 Estimations of tracer diffusivities and atomic mobilities

Zhong *et al*. (Zhong, Yang, & Liu, 2005) determined the activity of Mg as a function of concentration in the Mg-Al system by first principles calculations and compared the results with experimental data from Brown and Pratt (Brown & Pratt, 1970) at 710K and 660K. These calculations were found to be in good agreement with the experimental data and were utilized to estimate the tracer diffusion coefficient and atomic mobility of Mg and Al in the β-phase at the marker plane composition of Mg-62 at.% Al. Zhong *et*

al. determined the activity of Mg in the β-phase assuming it is a stoichiometric line compound. However, in this study, a small solubility range of ~2.5 at.% is clearly observed from the experimental concentration profiles as presented in Figure 15, and in accordance with the phase diagram in Figure 12. Using the maximum and minimum of the activity of Mg computed for the stoichiometric β-phase by Zhong *et al*. and the ~2.5 at.% solubility of the β-phase observed in this study, the activity of Mg at the temperatures of interest were linearly approximated as seen in Figure 29. Table 14 shows the estimated activities of Mg for the three experimental temperatures of this study.

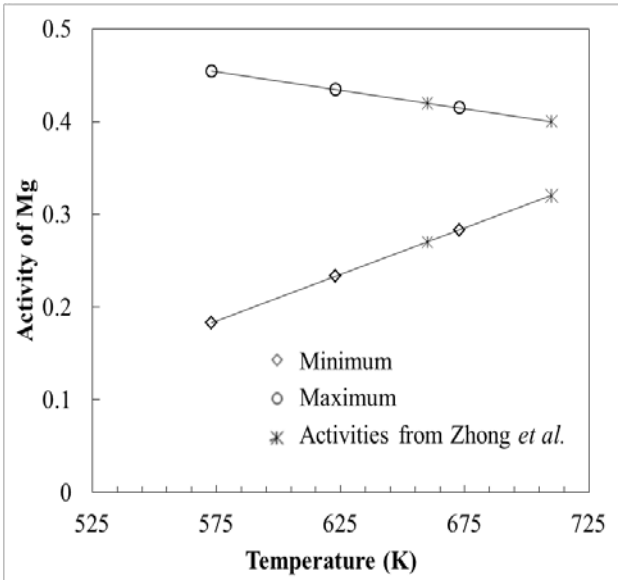

Figure 29: Estimates of the Mg activity in the β-Mg_2Al_3 phase, with solubility, as a function of temperature.

Table 14: Estimates of the activity of Mg, thermodynamic factor, Φ, tracer diffusion coefficient, D_i^*, and atomic mobiity, β_i in the β-Mg_2Al_3 phase at the approximate marker plane composition of 38 at.% Mg.

Temperature	Activity a_{Mg}	Thermo-dynamic factor, Φ	Tracer Diffusion Coefficient (m^2/s)		Mobilities (m/s-N)	
			D_{Al}^{β}	D_{Mg}^{β}	β_{Al}	β_{Mg}
673K	0.31	1.25	2.3×10^{-13}	1.5×10^{-14}	2.5×10^{7}	1.6×10^{6}
623K	0.21	1.5	5.9×10^{-14}	2.6×10^{-15}	6.6×10^{6}	3.0×10^{5}
573K	0.20	1.66	5.3×10^{-15}	5.0×10^{-16}	6.6×10^{5}	6.6×10^{4}

From the estimated activity of Mg in the β-Mg_2Al_3 phase presented in Figure 29, the thermodynamic factor (Darken, 1948), $\Phi = \delta\ln(a_i)/\delta\ln(N_i)$ was calculated as reported in Table 14. The estimated thermodynamic factors increase with decreasing temperature but are still relatively close to unity for each temperature. Then, tracer diffusion coefficients,D_i^*, for Al and Mg in the β-Mg_2Al_3 phase at the marker plane concentration of 38 at.% Mg were calculated using the simple expression (Darken, 1948), $D_i = D_i^*\Phi$, assuming negligible vacancy wind effects. Furthermore, the atomic mobility, β_i, of Al and Mg in the β-phase at the marker plane concentration was calculated using (Darken, 1948) $D_i = \beta_i RT\Phi$. These are reported in Table 14 also. The intrinsic diffusion coefficients in the β-phase at the marker plane composition of 38 at.% Mg were reported in Table 10. The mobility of Al in the β-phase at the marker plane concentration is higher than that of Mg.

5.2 Self- and impurity diffusion analysis

5.2.1 Aluminum impurity diffusion in magnesium

The impurity diffusion of aluminum in polycrystalline magnesium was measured via depth profiling with secondary ion mass spectroscopy. The calculated activation energy, from Figure 23, is 155 kJ/mole. To the author's knowledge, an impurity diffusion study of Al in Mg has not been reported, possibly due to the lack of availability of a suitable isotope tracer for Al. ^{26}Al is the only radioactive tracer for Al and is difficult and costly to obtain. Occasionally, indium (^{114}In) is used as a similar acting substitute for ^{26}Al; these two elements are in the same column on the periodic table of elements. Figure 30 shows the temperature-dependence of the Al impurity diffusion in Mg from this study in comparison to the impurity diffusion of ^{114}In in single crystal and polycrystalline Mg from Combronde and Brebec (Combronde & Brebec, Heterodiffusion de Ag, Cd, In, Sn et Sb dans le magnesiumg, 1972) and Lal (Lal, 1967), respectively. As evident from Figure 30, the magnitude of the diffusion coefficients is relatively similar for In and Al impurity diffusion in Mg, however the activation energy for Al impurity diffusion from this study is slightly higher. The diffusion coefficients and activation energies obtained from these experiments will be discussed further in Chapter 5.3 in comparison to the impurity diffusion extrapolations made in Chapter 5.1.4.

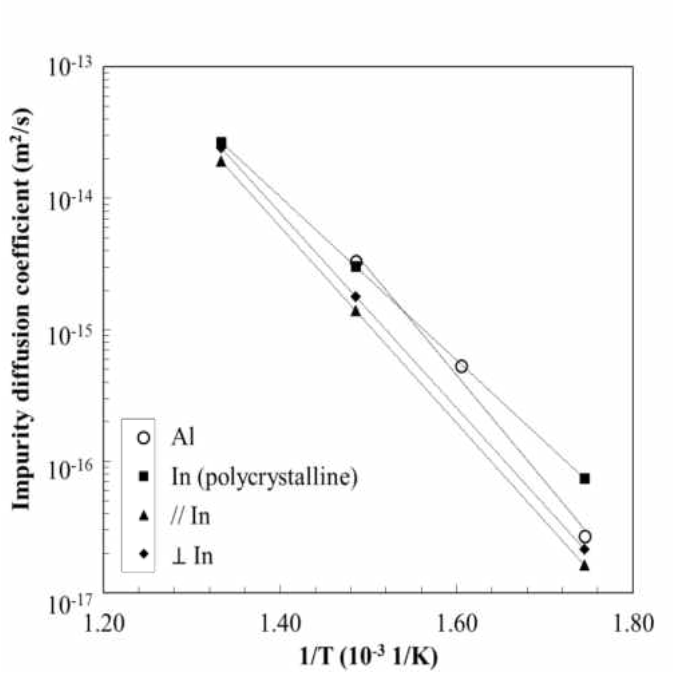

Figure 30: Impurity diffusion coefficient comparison for literature values of In in single crystal and polycrystalline Mg and the presently measured Al impurity diffusion in polycrystalline Mg. (In in single crystal Mg from (Combronde & Brebec, Heterodiffusion de Ag, Cd, In, Sn et Sb dans le magnesiumg, 1972) and in polycrystalline from (Lal, 1967)).

From Table 11, it can be readily observed that the impurity diffusion coefficient can be obtained to within ± 11% between different samples for the 573K sample and within ± 16.5% for the 623K samples which correspond to the lowest and highest standard deviations. These uncertainty values only encompass the calculations of the diffusion coefficient from the SIMS depth profile. Other sources of uncertainty, such as the accuracy of depth measurement of the sputtered crater via profilometery and estimation of the sputter rate, add to the uncertainty in calculating the diffusion coefficient. Under improved experimental conditions, such as having a much larger grain size in the Mg

substrate, or single crystal Mg, would decrease this uncertainty, especially at deeper depths (higher temperature specimens) where sputter roughening and atomic mixing due to SIMS is more of a concern.

5.2.2 Self-diffusion of the stable isotope ^{25}Mg in polycrystalline magnesium

Aforementioned, the calculated self-diffusion coefficients for ^{25}Mg in polycrystalline Mg with a grain size between 30 and 60 μm is higher by 1 to 1.5 orders of magnitude than reported literature values. The literature values of Mg self-diffusion are mainly in single crystals; one study was conducted in polycrystalline specimens with a grain size of ~1 mm (Shewmon & Rhines, 1954). There are several possible reasons for the discrepancy in the calculated values and the literature values:

- Sputter roughening due to broad grain size distribution leading to incorrect depth measurements.
- Grain boundary and microstructural effects (fast diffusion paths).
- Impurity levels in current specimens versus specimens from literature (current specimens are of higher purity).
- Recrystallization/grain growth due to some remaining stored internal energy after processing (Mg disks are from extruded rods).
- Experimental errors in measurements and data analysis.

It has been suggested that the most reliable measurements of diffusion coefficients utilizing SIMS are obtained from single crystal specimens, or polycrystalline specimens with very large grain sizes and significant crystallographic texture to ensure a constant sputtering rate. However, with smaller grain sizes, the sputtering roughening could be enhanced due to the sputter rate differing with crystallographic orientation. With multiple grains included in the raster area (sputter area) the roughening would increase as the depth of the crater increased. This roughening leads to an artificial broadening of the depth profile and thus, to a less accurate slope used to calculate the diffusion coefficients.

Another cause for the difference of the diffusion coefficient from literature values could be the grain boundary effects on the diffusion process. Grain boundaries are high diffusivity paths, meaning, atoms have higher mobility through grain boundaries due to the more defect oriented and "open" nature of grain boundaries. Grain boundary diffusion typically affects the diffusion process more strongly at temperatures below $0.6T_m$, where T_m is the melting point. The melting point of Mg is 923K, therefore ~554K is 0.6 of the melting temperature. Two of the specimens annealed in this study, the 573K and 523K specimens are close to this temperature. A characteristic sign of grain boundary contributions is a long "tail" at the end of the Ln(C) vs. x^2 profile. The thin film specimens annealed at 573K and 523K did display a somewhat noticeable tail, as seen in Figure 31. The tail portions of these profiles were not used in the calculation of the

diffusion coefficient; instead, the left-most linear portion traditionally corresponding to bulk or lattice diffusion was used.

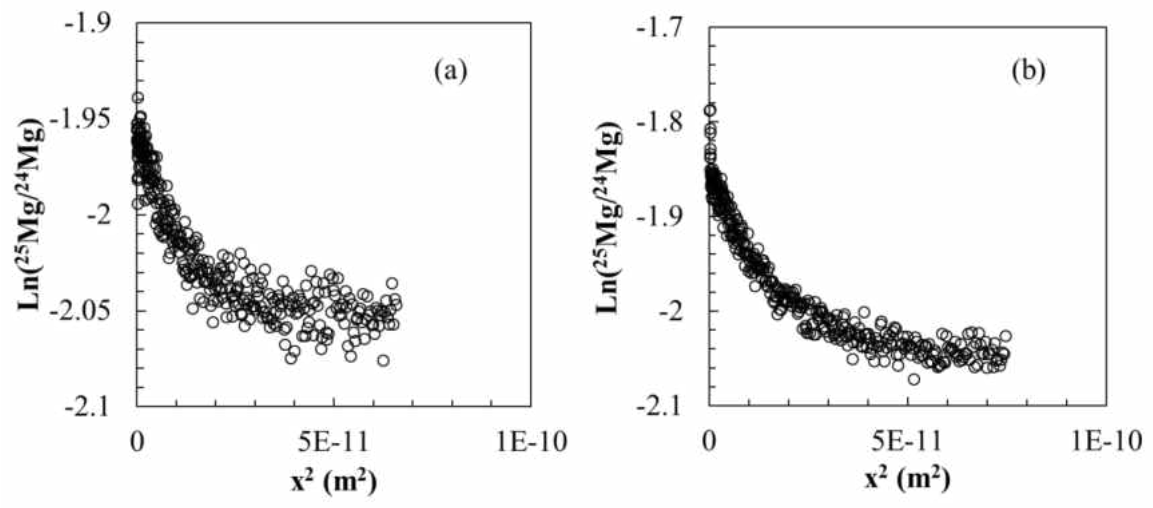

Figure 31: Natural logarithm of the $^{25}Mg/^{24}Mg$ isotope ratio versus distance squared plots showing possible grain boundary diffusion tails for (a) 573K for 240 minutes and (b) 523K for 720 minutes.

The literature values reported for Mg self-diffusion were obtained from radiotracer experiments where mechanical sectioning was employed to determine the concentration profile. The specimen preparation, diffusion annealing times and subsequent analysis for these experiments by both Shewmon (Shewmon & Rhines, Rate of Self-Diffusion in Polycrystalline Magnesium, 1954) (Shewmon, 1956) and Combronde and Brebec (Combronde & Brebec, Anisotropie d'autodiffusion du magnesium, 1971) were significantly short due to the short half-life (21.3 hours) of the

radioactive isotope, ^{28}Mg that was utilized. There could possibly be a significant experimental uncertainty associated with these experiments, leading to different values from those seen in this study.

5.3 General discussion of the interdiffusion and impurity diffusion analyses for the Mg-Al system

As stated previously, to the author's knowledge, there is no experimental report for Al impurity diffusion in Mg. A comparison of the experimentally measured Al impurity diffusion coefficients via SIMS to the impurity diffusion extrapolations and previously mentioned In impurity diffusion in Mg is shown in Figure 32. It is clear that the measured Al impurity diffusion coefficients are higher than those extrapolated from the interdiffusion data, however, the coefficients agree reasonably well at lower temperatures. It is also evident that the use of In as a diffusion substitute for Al is well founded, as its diffusivity is within the range between the extrapolated and experimentally measured values for Al impurity diffusion in Mg. It is also evident from the figure that the diffusion of Al in Mg is somewhat faster than that of Mg self-diffusion.

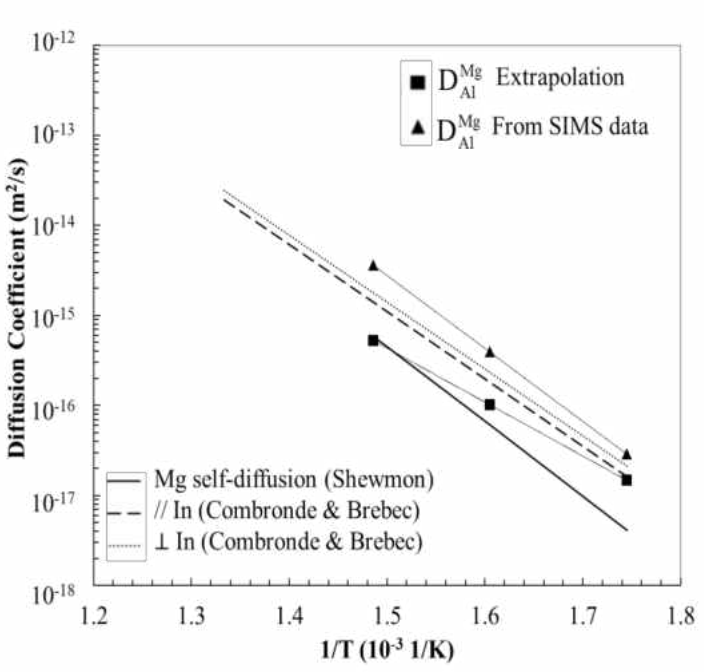

Figure 32: Impurity diffusion coefficient comparison for Al in Mg from experimental calculations and extrapolations from interdiffusion data, In impurity diffusion in Mg, and self-diffusion of Mg.

6 CONCLUSIONS

In this study, the intermetallic phase formation and growth, interdiffusion and intrinsic diffusion behavior in the Mg-Al binary system was investigated via solid-to-solid diffusion couples in the temperature range of 673-573K. The main observations from this interdiffusion study were:

- The formation of two intermetallic phases, β-Mg_2Al_3 and γ-$Mg_{17}Al_{12}$, of which, the β-phase formed a much thicker layer, had higher growth constants, higher interdiffusion coefficients, and lower activation energies for both growth and interdiffusion.
- Parabolic growth constants were determined for both intermetallic phases observed and activation energies for growth were calculated as 86 kJ/mole for the β-Mg_2Al_3 phase and 165 kJ/mole for the γ-$Mg_{17}Al_{12}$ phase.
- Concentration-dependent interdiffusion coefficients were determined with the Boltzmann-Matano analysis and the β-Mg_2Al_3 phase had the highest magnitude, followed by the γ-$Mg_{17}Al_{12}$ phase, the Al solid solution and the Mg solid solution.
- From the determination of average effective diffusion coefficients, activation energies for interdiffusion for the Al solid solution, β-Mg_2Al_3, γ-$Mg_{17}Al_{12}$, and Mg solid solution phases were calculated as ~105, 83, 123, and 187 kJ/mole, respectively.
- The Kirkendall marker plane was utilized to determine the intrinsic diffusion coefficients of Al and Mg in the β-Mg_2Al_3 at the approximate marker plane

composition of Mg-62 at.% Al. Al was determined to have the higher intrinsic diffusivity in this phase at the marker plane, however the activation energy for Al intrinsic diffusion, 112 kJ/mole was similar to that for Mg at 100 kJ/mole.

Additionally, estimates of the impurity diffusion coefficients of Mg in Al (ss) and Al in Mg (ss) were made and compared to available literature data with reasonable agreement. From the activity of Mg in the β-Mg_2Al_3 phase reported in literature, the thermodynamic factor was calculated to be close to unity. Estimations of the tracer diffusion coefficients and mobilities of Al and Mg in the β-Mg_2Al_3 phase at the marker plane concentration were carried out, showing both values to be higher for Al than for Mg.

The Al impurity diffusion in polycrystalline Mg via depth profiling with secondary ion mass spectrometry was also studied in the temperature range of 673-573K, utilizing the thin film method and thin film solution to the diffusion equation to extract the diffusion coefficient. The diffusion coefficient can be described by:

$$D_{Al}^{Mg} = 3.9x10^{-3} \exp\left(-\frac{155kJ}{mol}/RT\right) \ m^2/s.$$

The self-diffusion of the stable isotope ^{25}Mg in polycrystalline Mg was also investigated via the thin film method and measured with SIMS depth profiling. The values of the diffusion coefficient for this study in the temperature range of 523-673K were

significantly higher than those reported in literature. Possible reasons for this include sputter roughening and broadening of the depth profile due to an inconstant sputter rate resulting from a broad grain size distribution, higher purity specimens used in the current study versus the literature specimens, and possible grain boundary and other short circuiting diffusion effects. It is also possible that the reported literature values for the self-diffusion of the radioactive isotope ^{28}Mg in Mg contain significant sources of error due to the complex experimental set up and short half-life (21.3 hours) of the isotope.

APPENDIX: LIST OF RELATED PUBLICATIONS AND PRESENTATIONS

Publications:

1. S. Brennan, A.P. Warren, K.R. Coffey, Y.H. Sohn, N. Kulkarni, P. Todd, "Impurity Diffusion Studies of Aluminum in Magnesium," Magnesium Technology 2010, ed. By S.R. Agnew, N.R. Neelameggham, E.A. Nyberg, W.H. Sillekens, TMS, 2010, pp. 537-538.
2. S. Brennan, K. Bermudez, N. Kulkarni, Y.H. Sohn, "Growth Kinetics of γ-$Al_{12}Mg_{17}$ and β-Al_3Mg_2Intermetallic Phases in Mg vs. Al Diffusion Couple," Magnesium Technology 2011, ed. by W.H. Sillekens S.R. Agnew, N.R. Neelameggham, S.N. Mathaudhu, TMS, 2010, pp. 549-552.

Presentations:

1. Sarah Brennan, Andrew P. Warren, Kevin R. Coffey, Nagraj Kulkarni, Peter Todd, Yongho Sohn, Mikhael Klimov, Poster: "Tracer Diffusion Studies in Magnesium", Gordon Research Conference, Physical Metallurgy, Andover, NH August 2^{nd}-7^{th}, 2009.
2. N. S. Kulkarni, P.J. Todd, Y. Sohn, K. Coffey, and S. Brennan, "High Throughput Isotopic Diffusion Databases for Integrated Computational Materials Engineering," Presented at the 2009 AMD Lightweight Metals and Enabling Technologies Symposium, Detroit, Michigan, Oct. 13, 2009.
3. Sarah Brennan, Andrew P. Warren, Mikhail Klimov, Kevin R. Coffey, Yongho Sohn, Nagraj Kulkarni, Peter J. Todd, Poster: "Experimental Determination of Al, Zn and Mn Impurity Diffusion Coefficients in Magnesium", MS&T '09, Phase Stability, Diffusion Kinetics and Their Applications (PSDK-IV), Pittsburgh, PA October 25^{th}-29^{th}, 2009.
4. Sarah Brennan, Andrew P. Warren, Mikhail Klimov, Kevin R. Coffey, Yongho Sohn, Nagraj Kulkarni, Peter J. Todd, Presentation talk: "IMPURITY AND TRACER DIFFUSION STUDIES IN MAGNESIUM AND ITS ALLOYS", TMS 2010 Magnesium Technology 2010: Effects of Heat Treatment and Casting Process, Seattle, WA Feb. 14^{th}-18^{th}, 2010.
5. N. Kulkarni, P. Todd, Y.H. Sohn, K.R. Coffey, S. Brennan, J. Hunter, "Isotopic Diffusion Database for Mg ICME," Invited Presentation at the U.S. Automotive Materials Partnership Integrated Computational Materials Engineering (UAMP-IMCE) for

Magnesium Program Workshop, April 30-31, 2010, U.S. Council for Automotive Research (USCAR) LLC, Southfield, MI, USA.

6. Sarah Brennan, Katrina Bermudez, Nagraj Kulkarni, Yongho Sohn, “Interdiffusion in the Mg-Al system and Intrinsic Diffusion in β (Al_3Mg_2) Phase”, 2011 TMS Annual Meeting & Exhibition, Magnesium Technology 2011, San Diego, CA, Feb. 27th-Mar. 3rd, 2011.

LIST OF REFERENCES

Avedesian, M., & Baker, H. (1999). *Magnesium and Magnesium Alloys.* Materials Park, OH: ASM International.

Bamberger, M., & Dehm, G. (2008). Trends in the Development of New Mg Alloys. *Annu. Rev. Mater. Res. Vol. 38*, 505-533.

Boltzmann, L. (1894). Zur Integration der Diffusionsgleichung bei variablen Diffusionskoeffizienten . *Wien. Ann. Vol. 53*, 959.

Brown, J., & Pratt, J. (1970). The thermodynamic properties of solid Al-Mg alloys. *Metall. Trans. Vol. 1 No. 10*, 2743-50.

Brubaker, C., & Liu, Z. (2004). Diffusion couple study of the Mg-Al system . *Mg. Tech*, 229-34.

Bungardt, W. (1937). *Luftfahrforsch Vol. 14*, 204.

Cho, K., Sano, T., Doherty, K., Yen, C., Gazonas, G., Montgomery, J., et al. (2009). Magnesium Technology and Manufacturing for Ultra Lightweight Armored Ground Vehicles. *Proc. 2008 Army Science Conference*.

Combronde, J., & Brebec, G. (1971). Anisotropie d'autodiffusion du magnesium. *Acta Metall. Vol. 19*, 1393-99.

Combronde, J., & Brebec, G. (1972). Heterodiffusion de Ag, Cd, In, Sn et Sb dans le magnesiumg. *Acta Metall. Vol. 20 Issue 1*, 37-44.

Crank, J. (1975). *The Mathematics of Diffusion 2nd Ed.* Oxford: Oxford University Press.

Darken, L. (1948). Diffusion, Mobility and Their Interrelation through Free Energy in Binary Metallic Systems. *Trans. AIME Vol. 175*, 184-201.

Dayananada, M. (1993). Average Effective Interdiffsuion Coefficients in Binary and Multicomponent Alloys. *Defect and Diffusion Forum Vol. 95-98*, 521-36.

Dayananda, M. (1996). Average effective interdiffusion coefficients and the Matano plane composition. *Metall. Mater. Trans. A Vol. 27A*, 2504-2509.

Dayananda, M., & Kim, C. (1979). Zero-flux planes and flux reversals in Cu−Ni−Zn diffusion couples. *Metall. Mater. Trans. A Vol. 10A*, 1333-39.

Dow Chemical Company. (1982). *Fabricating with Magnesium, Dow Handbook.* Midland, MI: The Dow Chemical Company.

Dybkov, V. (2002). *Reaction Diffusion and Solid State Chemical Kinetics.* Kyiv: The IPMS Publications.

Fick, A. (1855). On liquid diffusion. *Philos. Mag. Vol. 10 Issue 63*, 30-39.

Fick, A. (1855). Ueber Diffusion. *Annalen der Phyik und Chemie Vol. 170 Issue 1*, 59-86.

Fujikawa, S. (1992). Diffusion in magnesium. *J. Hpn. Inst. Light Met. Vol. 42 No. 12*, 822-825.

Fujikawa, S., & Hirano, K. (1977). Diffusion of 28Mg in aluminum. *Mater. Sci. Eng. Vol. 27*, 25-33.

Fukuchi, M., & Watanabe, K. (1969, April). *Presented at the Spring Meeting of the Japan Institute of Metals*. Japan.

Funamizu, Y., & Watanabe, K. (1972). Interdiffusion in the Al-Mg System. *Trans. Jpn. Inst. Met. Vol 13*, 278-83.

Ganeshan, S., Hector Jr., L., & Liu, Z. (2010). First-principles study of self-diffusion in hcp Mg and Zn. *Comput. Mater. Sci. vol. 50 issue 2*, 301-307.

Gibbs, G. (1966). Diffusion Layer Growth in a Binary System . *J. Nucl. Mater. Vol. 20 No. 1*, 303-306.

Heumann, T. (1952). *Z. Phys. Chem. Vol. 201*, 168.

Heumann, T., & Kottmann, A. (1953). *Z. Metallk. Vol. 44*, 139.

Kajihara, M. (2004). Analysis of kinetics of reactive diffusion in a hypothetical binary system. *Acta Metall. Vol. 52*, 1193-1200.

Kidson, G. (1961). Some Aspects of the Growth of Diffusion Layers in Binary Systems. *J. Nucl. Mater. Vol. 3 No1*, 21-29.

Kirkendall, A. D. (1947). Zinc Diffusion in Alpha Brass. *Trans. AIME Vol. 171*, 130.

Kulekci, M. (2008). Magnesium and its alloys applications in automotive industry. *Int. J. Adv. Manuf. Tech. Vol. 39*, 851-65.

Lal, K. (1967). *CEA Report R*, 3136.

Lal, K. (1967). *CEA Report R 3136*, 54.

Lundy, T., & Murdoch, J. (1962). Diffusion of Al26 and Mn54 in Aluminum. *J. Appl. Phys. Vol. 33 No. 5*, 1671-73.

Luo, A. (2002). Magnesium: Current and potential automotive applications. *JOM Vol. 54 No. 2*, 42-48.

Manning, J. (1967). Diffusion and the Kirkendall shift in binary alloys. *Acta. metall. Vol. 15 Issue 5*, 817-826.

Manning, J. R. (1968). *Diffusion Kinetics for Atoms in Crystals.* Princetone: van Norstrand.

Matano, C. (1933). On the relation between the diffusion-coefficients and concentrations of solid metals (the nickle-copper system). *Japanese Journal of Physics Vol. 8*, 109-113.

Mehrer, H. (2007). *Diffusion in Solids: Fundamentals, Methods, Materials, Diffusion-Controlled Processes.* Berlin: Springer.

Mordike, B., & Ebert, T. (2001). Magnesium: Properties-applications-potential. *Mater. Sci. Eng. A Vol. 302*, 37-45.

Moreau, G., Cornet, J., & Calais, D. (1971). *J. Nucl. Mater. Vol. 38 Issue 2*, 197-202.

Okamoto, H. (1998). Al-Mg (Aluminum-Magnesium). *J. Phase Euilib. Vol. 19* , 598.

Pavlinov, L., Gladyshev, A., & Bikov, V. (1968). *Fiz. Met. Metalloved Vol. 26 Issue 5*, 823.

Petuskey, W. (1983). Diffusion Analysis Using Secondary Ion Mass Spectroscopy (SIMS). *Nontraditional Methods in Diffusion* (pp. 179-203). Philadelphia: The Meallurgical Society of AIME.

Philibert, J. (1991). *Atom Movements Diffusion and Mass Transport in Solids.* France: Les Editions de Phusique.

Pretorius, R., Marais, T., & Theron, C. (1993). Thin film compound phase formation sequence: An effective heat of formation model. *Mater. Sci. Rep. Vol. 10*, 1-83.

R. Urnance, F. R. (2002). Market Model Simulation: The Impact of Increased Automotive Interest in Magnesium. *JOM Vol. 54 No. 8*, 25-33.

Samson, S. (1965). The Crystal Structure of the Phase β-Mg2Al3. *Acta Cryst. Vol. 19*, 401-413.

Sauer, F., & Freise, V. (1962). Diffusion in binaren Gemischen mit Volumenanderung. *Z. Elektrochem Vol. 66*, 353.

Shewmon, P. (1956). *Trans. AIME Vol. 206*, 918.

Shewmon, P. (1989). *Diffusion in Solids.* Warrendale: The Minerals, Metals & Materials Society.

Shewmon, P., & Rhines, F. (1954). Rate of Self-Diffusion in Polycrystalline Magnesium. *Trans. AIME Vol. 250*, 1021-25.

Tanguep Njiokep, E., Salomon, M., & Mehrer, H. (2001). Growth of Intermetallic Phases in the Al-Mg System . *Defect Diffusion Forum Vol. 194-199*, 1581-86.

Urbance, R. J., Field, F., Kirchain, R., Roth, R., & Clark, J. P. (2002). Market Model simulation: The Impact of Increased Automotive Interest in Magnesium. *JOM*, 25-33.

Wagner, C. (1969). The Evaluation of Data Obtained with Diffusion Couples of Binary Single-Phase and Multiphase Systems. *Acta Metall. Vol. 17*, 99-107.

Xu, Y., Chumbley, L., Weigelt, G., & Laabs, F. (2001). Analysis of interdiffusion of Dy, Nd, and Pr in Mg. *J. Mater. Res. Vol. 16 No. 11*, 3287-92.

Ye, H., & Liu, X. (2004). *J. Mater. Sci. Vol 39*, 6153-71.

Zaludova, N. (2005). Mg-RE Alloys and Their Applications. *WDS'05 Proceedings of Contributed Papers, Part III*, (pp. 643-648).

Zhang, X., Kevorkov, D., & Pekguleryuz, M. (2010). *J. Alloys Compd. Vol. 501*, 366-70.

Zhao, H., Qin, G., Ren, Y., Pei, W., Chen, D., & Guo, Y. (2010). *Journal of Alloys and Compounds*, In Press.

Zhong, Y., Yang, M., & Liu, Z. (2005). Contribution of first-principles energetics to Al-Mg thermodynamic. *CALPHAD: Comput. Coupling Phase Diagrams Thermochem. Vol. 29*, 303-11.